Universidade de Vigo

TECHNISCHE UNIVERSITÄT WIEN
Vienna University of Technology

DIPLOMA THESIS

Linear Viscelastic UMAT Development in the Frequency Domain

Jorge Regueiro Penado

Vienna, June 2015

Institut für Leichtbau und Struktur-Biomechanik
Technische Universität Wien

Departamento de Diseño en la Ingeniería
Universidade de Vigo

Supervisor 1: Heinz Petterman, TU Wien
Supervisor 2: José Antonio Pérez García, UVigo

Acknowledgment

I would like to thank Dr. Heinz Pettermann for the supervision of my thesis. Not just for his patience and unconditional support with a student that practically had no previous knowledge of FEM, but also for his commitment and advice every time I needed, I will always be indebted to you. My most sincere thanks also to Prof. José Antonio Pérez García and Dr. Helmut Böhm for the possibility to come to Vienna to do my final project.

I wish to acknowledge my university colleagues from Universidade de Vigo, for that constant combination between competition and support that have made me grow this far as engineer. Special mention deserve Alejandro Alonso, Alejandro Vázquez and Borja Boyano, specially the latter for putting up with my failures and successes all these year in the ILSB.

Thanks also to my home city friends for standing by my side all these years. Particularly to Marco Antonio Coto and Iago Diéguez, they have been my main support in good and bad times. I will always be there for you. I do not forget Aida Santos for making me become the man I am, I am deeply indebted to you too.

Por último, por supuesto gracias a mis padres y hermana, por su esfuerzo diario para hacer esto posible y por no dudar jamás de mi, sin ellos y su aliento nunca hubiera llegado a la mitad de lo que soy ahora. Va por vosotros.

J.R.P.

Abstract

The importance of simulation in engineering research is undeniable, the fact that its application needs much less money than physical tests reduces research and development costs drastically. The present thesis deals with the development and implementation of a constitutive model of different anisotropic, viscoelastic material behaviour for carrying out steady state dynamics simulations. The types of anisotropy studied are concretely cubic anisotropy and orthotropy, which can be easily simplified to transversal isotropy.

For achieving this objective, the most important theoretical concepts are developed, ranging from elasticity and linear viscoelasticity theories to some Finite Element Method techniques.

The constitutive model will be programmed in an Abaqus UMAT subroutine. This UMAT allows the implementation of the material constitutive law in Abaqus commercial software to carry out the desired frequency domain studies, or, more precisely, to predict how the material behaves under the effect of harmonic excitaton.

The material input data for the UMAT is obtained through simulations applied to unit cells with the structure and material properties under study. By these unit cell and with periodic boundary conditions, an infinitely repeating pattern of the cellular architecture is simulated.

Furthermore, the quality of the UMAT predictions will be intensely tested through different simulations at different frequencies. Such simulations will be applied to both the inhomogeneous unit cell and an homogenous unit cell whith the homogeneized input data applied through the UMAT. The results from both simulations will be compared in order to test the accuracy of the simulations when the UMAT is applied.

Some UMAT applications are also dealt. On one side, the UMAT for cubic anisotropy will be applied to a cubic finite model with different material principal directions. On the other hand, a DMA model is developed and implemented to simulate a four-layered composite with different configurations in the transversally isotropic layer orientations.

Resumen

En ingeniería, la importancia de la simulación por ordenador en investigación y desarrollo es innegable, el motivo es básicamente que su aplicación es mucho más económica que la de test reales, por lo cual reduce enormemente los costes del proceso. El presente proyecto consiste en el desarrollo y aplicación de distintos modelos constitutivos de materiales anisotrópicos y linealmente viscoelásticos, para ser aplicados a simulaciones de "steady-state dynamics", i.e. simulaciones de estado estacionario en oscilaciones forzadas.

Para alcanzar dicho objetivo, están incluidos los conceptos teóricos más importantes para su desarrollo, desde los conceptos de elasticidad y viscoelasticidad lineal hasta las técnicas de elementos finitos empleadas.

La ley constitutiva de los distintos tipos de materiales considerados será programada en una subrutina tipo UMAT. Un UMAT permite la implementación de dicha ley constitutiva en Abaqus, permitiendo el empleo en simulaciones de materiales que de otra forma no sería posible, para llevar a cabo estudios sobre el material en el dominio de la frecuencia, i.e. cómo se comportará el material al ser sometido a cargas periódicas.

Los datos de entrada para el UMAT son obtenidos por medio de diferentes simulaciones aplicadas a celdas unitarias con la correspondiente estructura y propiedades materiales bajo estudio. Con esta celda unitaria, sometida a condiciones de contorno periódicas, se simula una estructura infinita compuesta por la celda unitaria repetida infinitamente a lo largo del espacio, con ello se obtienen las propiedades medias del material considerado.

Además, la calidad de las predicciones realizadas por los UMAT será testeada de forma intensiva a través de distintos test a diferentes frecuencias. Dichos test serán aplicados a ambas, la celda unitaria no homogénea y la celda homogénea con las propiedades materiales homogeneizadas, introducidas en Abaqus a través del UMAT. Los resultados de ambas simulaciones serán comparados con el fin de comprobar la precisión de los resultados generados tras la aplicación del UMAT.

También están incluidas en el proyecto algunas aplicaciones del UMAT. Por un lado, el UMAT de anisotropía cúbica será aplicado a un modelo cúbico finito orientado en distintas direcciones. Además, ha sido desarrollado un modelo de DMA, i.e. "Dynamic Mechanical Analysis", y

ha sido implementado con un composite laminado de cuatro capas, cada una con propiedades de isotropía transversal, con distintas configuraciones en la disposición y orientación de la dirección principal de las láminas que componen la plancha.

Contents

Chapter 1

Introduction

As the objective of the present thesis is the simulation of different anisotropic materials in the frequency domain, some general aspects of both concepts are specified in this chapter.

1.1 Composite materials

Composite materials or composites are materials made from two or more constituent materials with significantly different physical or chemical properties that, when combined, produce a material with different characteristics from the individual components. The individual components remain separate and distinct within the final structure.

1.1.1 General properties

In comparison to common materials used today such as metal and wood, composites can provide a distinct advantage. One driver and advantage in the adoption of composites is the lightweight properties. In transportation, less weight equates to more fuel savings and improved acceleration. In sporting equipment, lightweight composites allow for longer drives in golf, faster swings in tennis, and straighter shots in archery. While in wind energy, the less a blade weighs, the more power the turbine can produce. The vast range of materials that can be combined turns into a huge variety of composites with very different properties and applications.

For example, in the context of this work, a fiber-reinforced thermoplastic matrix mainly presents high stiffness with a very reduced weight, so it can resist high loads in the fiber di-

rection without making the system much heavier, which means energy efficiency for the system it takes part, e.g. a vehicle. In consequence of the different behavior in fiber and transverse direction, this example is a case of an anisotropic material.

1.1.2 Classification of composites

Composite materials are commonly classified in two distinct levels, on the basis of matrix phase and on the reinforcement shape.

On the basis of matrix phase, composites can also be classified into *metal matrix composites* (MMCs), *ceramic matrix composites* (CMCs) and *organic matrix composites* (OMCs). The latter is generally assumed to include two classes of composites, namely *polymer matrix composites* (PMCs) and carbon matrix composites commonly referred to as *carbon-carbon composites*. The second level of classification refers to the reinforcement form, there are three types. *Fiber-reinforced composites* are composed of fibres embedded in matrix material. Such a composite is considered to be a discontinuous fiber or short fiber composite if its properties vary with fiber length. On the other hand, when the length of the fibre is such that any further increase in length does not further increase in the elastic modulus of the composite, the composite is considered to be continuous fiber reinforced. Fibers are small in diameter and when compressed axially, they bend easily although they have very good tensile properties. Another type are *laminar composites*,which are composed of layers of materials held together by the matrix. Sandwich structures fall under this category. Finally, *particle-reinforced composites* are composed of particles distributed or embedded in a matrix body. The particles may be flakes or in powder form. Concrete and wood particle boards are examples of this category.

1.1.3 One composite example: cellular materials

Cellular materials are those that contain many air cells or voids (either open or closed, or both) dispersed throughout the mass. The fundamental property is relative density, i.e. the ratio of the apparent mass density of the cellular material to the mass density of the base material, which in case of cellular materials is typically low (less than 0.3).

These materials are widespread in nature, like in cork or cancellous bone (figure 1.1) which

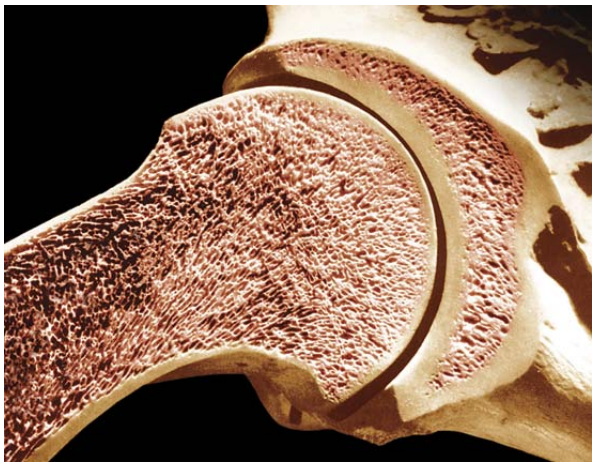

Figure 1.1: Example of cellular material: humerus cancellous bone. [15]

is found in most areas of bone that are not subject to great mechanical stress like at the ends of long bones. Furthermore, cellular materials are also in food, like in bread or chocolate. However, they are less explored, less well understood and worse documented. Recently, they have gained increased importance in engineering and bio medical applications, taking importance in industry, like in honeycombs, prosthesis or lightweight structures.

Their particular properties are governed by the internal cellular architecture and the material they are made of, leading to a tremendous variability and complexity. This high variability yields to such different applications, i.e. in some cases we have relatively poor structural properties, e.g. in thermal insulation or packaging, and in others we look for high stiffness with low density, e.g. in aerospace industry.

A better understanding of the relation between architecture and cellular material properties is required for service-oriented selection of existing materials. Moreover, such knowledge is the basis for tailoring man made materials by designing them adequately to show desired properties. [3][11]

Typically, cellular materials can be divided into three types: two-dimensional polygon arrangements; three-dimensional arrangements, which are generally referred to as foams and can be also divided into open-cell and closed-cell structures. The base material can be present only in the cell edges, which would be the case of open-cell materials, or it can take a spatial distribution in a way that each cell form a confined space, which is the case of closed-cell structures. For engineering applications mainly foams are used, i.e. polymeric, ceramic or metallic foams.

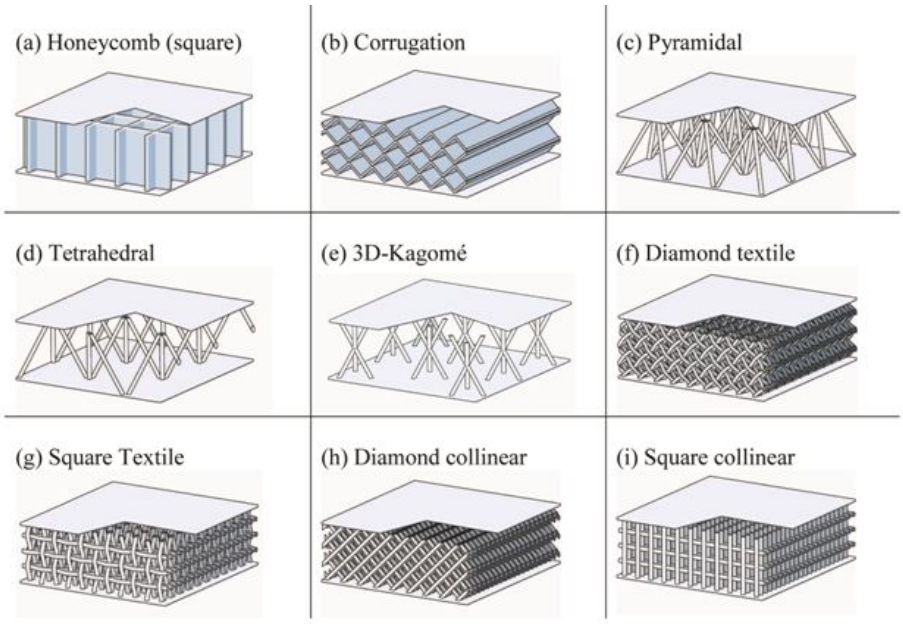

Figure 1.2: Different arrangements of cellular materials. [16]

Some examples of such cellular materials are given in figure 1.2.

1.1.4 Continuous fiber reinforced materials

Fiber reinforced composites are materials composed of fibers, which are generally the reinforcement and the main source of strength, and the matrix, which 'glues' all the fibers together in shape and transfers stresses between the reinforcing fibers. Some examples can be carbon or glass-fiber composites.

Most matrices are made of resins for their wide variation in properties and relatively low cost, e.g. polyester, polyamide or epoxy.

Reinforcing fibers are normally made of metals, ceramics, glasses, or polymers. The arrangement or orientation of the fibers relative to one another, the fiber concentration, and the distribution have a significant influence on the strength and other properties of fiber-reinforced composites. In the case of continuous fiber reinforcement, the fibers have a ratio length to transversal surface really high. This high ratio makes possible to assume the composite to behave as if the fibers were infinitely long.

1.2 Frequency domain viscoelastic behavior simulation

Many materials in nature and engineering present in greater or lesser extent viscoelastic behaviour, and they are loaded under periodic loads, e.g. vibrations in a vehicle, so their simulation in the frequency domain takes strong importance.

1.2.1 Material constitutive model and homogenization

A material constitutive model is a mathematical description of the material behavior. The developing of such material constitutive laws takes huge importance in simulation, one of the advantages is that it allows the homogenization of complex material arrangements, reducing not only the effort in meshing, but also the number of elements needed to accurately predict the overall behavior. In consequence, it reduces the computation time and the required resources incredibly.

In addition, all we need for applying these constitutive models to simulations are the correspondent material parameters. To obtain them, real tests can be carried out, but they are expensive, hard to implement and the material must be available, which is not always possible. Hence, Finite Element Method or simply FEM models are generally a good alternative. With FEM it is possible to predict the needed material properties from different simple load tests applied to a small, significative material portion, with relatively low computer requirements. The required material tests to get such properties are not unique and the minimum number of them that is needed to fully describe the material behaviour depends on each material under study.

Some viscoelastic constitutive models have been set in the time domain, i.e. to study how they behave under different types of loading or unloading periods of time, e.g. [26]. The implementation of viscoelastic constitutive models in the frequency domain is a new possibility in Abaqus software. In consequence, there has been not a very deep insight in its developing. The development of such a material law to simulate different viscoelastic anisotropic materials in the frequency domain, is the objective of the present thesis.

Chapter 2

Material behavior

In this chapter linear elastic deformation and linear viscoelastic behavior will be dealt with, as their combination compose the reaction mechanism to loading of the different anisotropic materials modeled in this thesis.

2.1 Linear elasticity

Solid objects will deform when forces are applied on them. Elasticity is the tendency of solid materials to return to their original shape after being deformed.

In engineering the amount of elasticity of a material is determined by two types of material parameter. The first type of material parameter is called a modulus, which measures the amount of force per unit area (stress) needed to achieve a given amount of deformation or strain. The second type of parameter measures the elastic limit, which is the stress beyond which the material no longer behaves elastic and permanent deformation of the material will take place.

With the assumption of small strains, which means that they do not exceed 5%, many elastic materials exhibit linear elasticity and can be described by a linear relation between stress and strain: the so-called Hooke's law, which in one-dimension stands for [18]:

$$\sigma = E\epsilon \quad , \tag{2.1}$$

with E as Young's modulus, ϵ as the strain and σ as the stress. Hooke's law for elastic materials

can also be written in terms of a compliance J:

$$\epsilon = J\sigma \quad . \tag{2.2}$$

Consequently, the elastic compliance, J, is the inverse of the Young's modulus, E :

$$J = \frac{1}{E} \quad . \tag{2.3}$$

2.2 Viscoelasticity

Most solid materials are described, for small strains, by Hooke's law of linear elasticity: stress σ is proportional to strain, as we could see in equation (2.1).

In contrast to elastic materials, a viscous fluid under shear stress obeys

$$\sigma = \eta \frac{\mathrm{d}\epsilon}{\mathrm{d}t} \tag{2.4}$$

with η as the viscosity and t as time.

In consequence, viscous materials, like honey, resist shear flow and strain linearly with *time*, t, when a stress is applied. On the other hand, elastic materials deform in such case and return to their original state once the stress is removed. In reality, materials deviate from Hooke's law in various ways, for example, by exhibiting viscoelasticity, which is the property of materials that exhibit both viscous and elastic characteristics when undergoing deformation and exhibit time-dependent strain or stress. Whereas elasticity is usually the result of bond stretching along crystallographic planes in an ordered solid, viscosity is the result of the diffusion of atoms or molecules inside an amorphous material. [20]

The previous statement yields from the stress–strain curve, which is obtained by applying a constant rate of strain to a bar of the material. If the material is linearly elastic, the curve is a straight line with a slope proportional to the elastic modulus (the thick line in the right diagram in figure 2.1). For a sufficiently large stress (the yield stress σ_y), the material yields as shown in the right plot of figure 2.1. This is a threshold phenomenon. A linear viscoelastic material, by contrast, gives rise to a curved stress–strain plot (the left diagram in figure 2.1) [18].

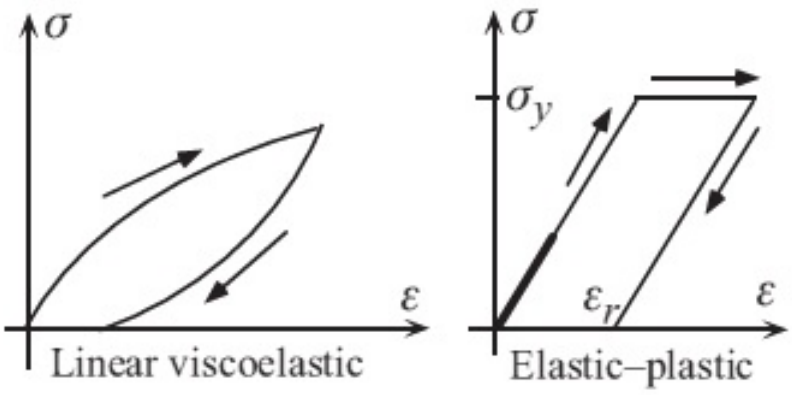

Figure 2.1: Stress-strain plots for a linear viscoelastic and a elastic-plastic material. [18]

The reason for this rise is that during constant strain rate deformation, both time and strain increase together. The viscoelastic material is sensitive to time. Consequently, the curve on the left becomes steeper if the strain rate is increased.

When testing and describing viscoelastic materials, it is preferable to apply a step strain or step stress in time rather than a ramp (constant rate of strain) because the effect of time is then isolated from any nonlinearity. The response to step strain is stress relaxation, and the response to step stress is creep.

2.2.1 Transient properties: creep and relaxation

These two properties take importance only in the time domain, which is out of the objectives of the thesis, but their explanation is important to understand how a viscoelastic material actually behaves.

Creep

Creep is a progressive deformation of a material under constant stress. In one dimension, suppose the history of stress σ as it depends on time t to be a step function with the magnitude σ_0, beginning at time zero:

$$\sigma(t) = \sigma_0 H(t) \quad , \tag{2.5}$$

where $H(t)$ is the unit Heaviside step function defined as:

$$H(t) = \begin{cases} 0 & \text{if} \quad t < 0 \quad . \\ 1/2 & \text{if} \quad t = 0 \quad . \\ 1 & \text{if} \quad t > 0 \quad . \end{cases} \tag{2.6}$$

The strain $\epsilon(t)$ in a viscoelastic material will increase with time. The ratio

$$J(t) = \frac{\epsilon(t)}{\sigma_0} \quad , \tag{2.7}$$

is called the *creep compliance*. In linear viscoelastic materials, the creep compliance is independent of stress level. The intercept of the creep curve on the strain axis is described by some authors to instantaneous elasticity. It is just a theoretical parameter, as no load can be physically applied instantaneously. If the load is released at a later time, the strain will exhibit recovery or a progressive decrease of deformation. Strain in recovery, referring to viscoelasticity, will approach zero. This recovery phase is not included in equations (2.5) and (2.7) for simplicity.

The creep response in figure 2.2 is shown beginning at the same time as the stress history, which is the cause, this follows from the physical concept of causality, that is, the effect does not precede the cause, and the same happens with the recovery phase when the stress is released. It is also appreciable in this figure that the viscoelastic behavior is a combination of both elastic and viscous behaviour.

Relaxation

Stress relaxation is the gradual decrease of stress when the material is held at constant strain. If we suppose the strain history to be a step function of value ϵ_0 beginning at time zero:

$$\epsilon(t) = \epsilon_0 H(t) \quad , \tag{2.8}$$

the stress $\sigma(t)$ in a viscoelastic material will decrease as shown in figure 2.3. The ratio

$$E(t) = \frac{\sigma(t)}{\epsilon_0} \quad , \tag{2.9}$$

is called the *relaxation modulus*. In linear materials, it is independent of strain level, so $E(t)$

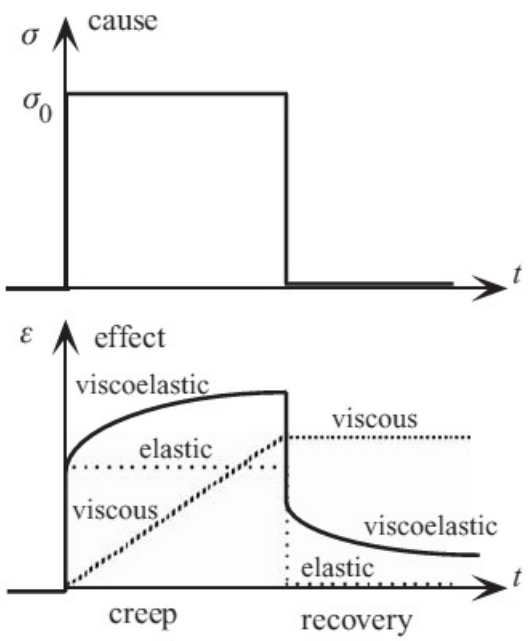

Figure 2.2: Creep and recovery. Stress σ and strain ϵ versus time t. [18]

is a function of time alone. So if we compare equation (2.9) and equation (2.7) we can appreciate that the creep compliance is not the inverse of the relaxation modulus.

Associated material parameters

Creep and relaxation can occur in shear as well as in volumetric deformation. The relaxation function for shear stress is called $G(t)$. For volumetric deformation, the instantaneous bulk modulus is called K_0 . A corresponding relaxation function $K(t)$ may be defined as in equation (2.9), but with the stress and strain with his hydrostatic counterparts. A similar distinction is made in the creep compliances, $J_G(t)$ for creep in shear, $J(t)$ for creep in extension, and $J_K(t)$ for creep in volumetric deformation.

A distinction may be made between aging and non-aging materials: in aging materials, properties change not only with time after we apply a stress or strain, but also with the time following the formation or transformation of the material. Concrete, for example, is an aging material. This thesis deals exclusively with non-aging materials.

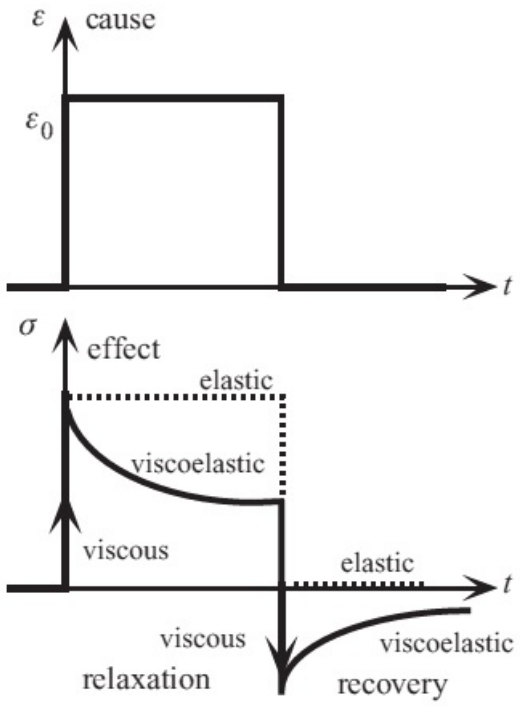

Figure 2.3: Relaxation and recovery. [18]

2.2.2 Dynamic response to sinusoidal load

The response of linear viscoelastic materials to sinusoidal load is developed in this section, and this response is referred to as dynamic. The dynamic behavior is of interest because viscoelastic materials are used in situations in which the damping of vibration or the absorption of sound is important. The frequency of the sinusoidal load on an object or structure may be so slow that inertial terms do not appear (the subresonant regime), or high enough that resonance of structures made of the material occurs. Oscillatory stress and strain histories are represented by sinusoid functions.

Suppose the strain $\epsilon(t)$ is varying sinusoidally in time t, as shown in figure 2.4:

$$\epsilon(t) = \epsilon_0 \sin(2\pi f t) \quad , \tag{2.10}$$

in which t is time, ϵ_0 is the amplitude and f is the frequency (in cycles per second or Hertz, abbreviated Hz). The reaction stress generated by such a strain of a linear viscoelastic material is also sinusoidal in time, but the stress will be advanced in phase by a phase angle δ, so the

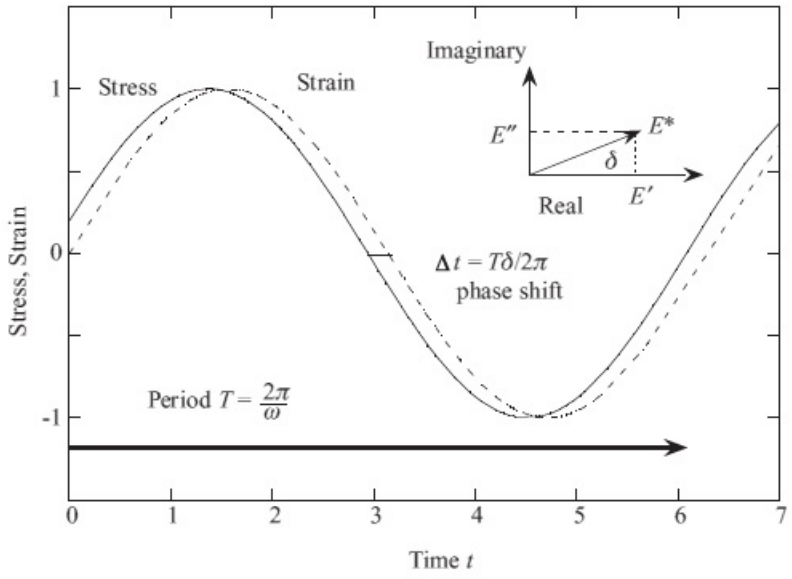

Figure 2.4: Stress and strain versus time, with a phase shift δ. [18]

stress caused by the strain of equation (2.10) takes the form

$$\sigma(t) = \sigma_0 \sin(2\pi f t + \delta) \quad . \tag{2.11}$$

The period T of the waveform is the time required for one cycle: $T = 1/f$. As is possible to appreciate in figure 2.4 The phase angle is related to the time lag Δt between the sinusoids by $\delta = 2\pi\Delta t/T$.

In a plot of the two waveforms, the sinusoids are shifted with respect to each other on the time axis as we can see in figure 2.4. Recall that the cosine function is $\pi/2$ radians out of phase with the sine function. Sinusoidal functions that represent oscillatory quantities in which phase is important are commonly written in *complex exponential notation.* [17]

As a result of the phase lag between stress and strain, the dynamic stiffness can be treated as a complex number E^* .

$$\frac{\sigma(t)}{\epsilon(t)} = E^* = E' + \imath E'' \quad , \tag{2.12}$$

where $\imath = \sqrt{-1}$. E' is the component of the stress–strain ratio in phase with the applied stress, and its called the *storage modulus*; E'' is the component 90^o out of phase and its called the *loss*

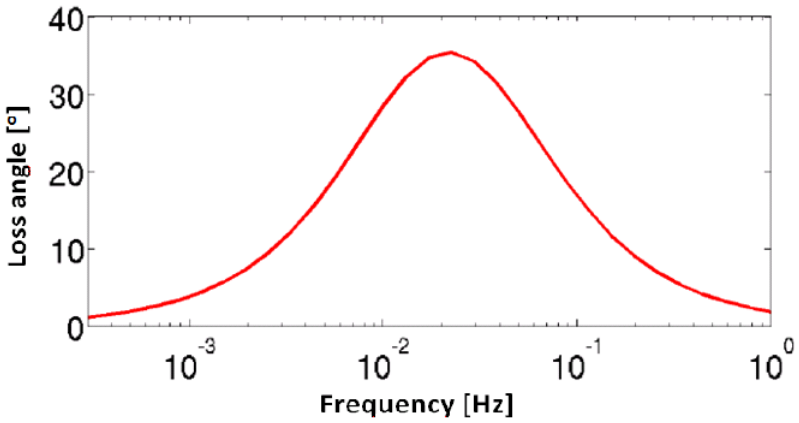

Figure 2.5: Loss angle in function of frequency example [10]

modulus.

The loss angle δ is a dimensionless measure of the viscoelastic damping of the material or the internal friction. The dynamic functions E', E'', and δ depend on frequency. The tangent of the loss angle is called the loss tangent: $\tan\delta$, and it stands for:

$$\tan\delta(f) = \frac{E''(f)}{E'(f)} \quad . \tag{2.13}$$

In an elastic solid, $\tan\delta = 0$. [18]

Considering the frequency dependency of the loss tangent that can be seen in figure 2.5, the loss angle takes value zero when the frequency tends to zero, as it would be a static loading case, but also when the frequency tends to infinity, as for these frequencies the relaxation modulus tends to the short term elastic modulus E_0, which has no loss angle. It takes a maximum value at a frequency value that depends on the material under study. [10]

2.2.3 Analytical solution procedure

Taking into account that the loss modulus of the viscoelastic material leads to one sort of damping, we can reduce the problem of the viscoelastic, periodically loaded structure stated in the previous section to a differential equation given by:

$$m\ddot{u} + \gamma\dot{u} + ku + F = 0 \quad , \tag{2.14}$$

where m is the *mass* of the system, u is the *displacement*, being $\dot{u}$ and $\ddot{u}$ its first and second derivatives respectively, γ is the associated *damping coefficient*, k is the stiffness of the system and F is the *applied force*.

If the force F in equation (2.14) is periodic or, more generally, if we can express it as

$$F = \bar{F}\exp(\alpha t) \quad , \tag{2.15}$$

where the phase angle αt, with α

$$\alpha = \alpha_1 + \imath\alpha_2 \quad , \tag{2.16}$$

and the amplitude $\bar{F}$

$$\bar{F} = \bar{F}_1 + \imath\bar{F}_2 \quad , \tag{2.17}$$

are complex. Then a general solution can be written in a similar way as in the previous section, but this time in terms of displacements

$$u = \bar{u}\exp(\alpha t) \quad . \tag{2.18}$$

Substituting the above in equation (2.14) gives

$$(\alpha^2 m + \alpha\gamma + k)\,\bar{u} = \bar{k}\bar{u} = -\bar{F} \quad . \tag{2.19}$$

The solution is thus precisely of the same form as that used for static problems, see equation (2.1), but now, however, has to be determined in terms of complex quantities. Computation can be carried out in terms of real numbers, by

$$\begin{aligned} \exp(\alpha t) &= \exp(\alpha_1 t)[\cos\alpha_2 t + \imath\sin\alpha_2 t] \\ \bar{F} &= \bar{F}_1 + \imath\bar{F}_2 \\ \bar{u} &= \bar{u}_1 + \imath\bar{u}_2 \end{aligned} \tag{2.20}$$

in which α_1, α_2, $\bar{F}_1$,$\bar{F}_2$, $\bar{u}_1$ and $\bar{u}_2$ are real quantities. Inserting equations (2.20) in equation (2.19) we have

$$\begin{pmatrix} (\alpha_1^2-\alpha_2^2)m+\alpha_1\gamma+E & -2\alpha_1\alpha_2 m-\alpha_2\gamma \\ -2\alpha_1\alpha_2 m-\alpha_2\gamma & -(\alpha_1^2-\alpha_2^2)m-\alpha_1\gamma-E \end{pmatrix} \begin{pmatrix} \bar{u}_1 \\ \bar{u}_2 \end{pmatrix} = - \begin{pmatrix} \bar{F}_1 \\ -\bar{F}_2 \end{pmatrix} \quad , \tag{2.21}$$

which forms a system in which all quantities are real and from which the response to any periodic input can be determined by direct solution. With periodic input the solution is not sensitive to the initial conditions and the above solution represents the finally established response [32], which is what we get in steady state dynamics simulations.

2.2.4 Mechanical viscoelasticity models

Among the simplest transient response functions are those that involve exponentials. In relaxation, we may consider

$$E(t) = E_0 e^{-t/\tau_\mathrm{r}} \quad , \tag{2.22}$$

with τ_r called the *relaxation time* and E_0 the instantaneous modulus. In creep, the corresponding relation is

$$J(t) = J_0(1-e^{-t/\tau_\mathrm{c}}) \quad , \tag{2.23}$$

with τ_c called the *creep* or *retardation time* and J_0 the instantaneous compliance. Exponential response functions arise in simple discrete mechanical models composed of springs, which are perfectly elastic, see equation (2.1) and dashpots, which are perfectly viscous, see equation (2.4). The dashpot may be envisaged as a piston–cylinder assembly in which motion of the piston causes a viscous fluid to move through an aperture.

The Kelvin-Voigt model

The Kelvin-Voigt model consists of a spring and dashpot in parallel, so that they both experience the same deformation or strain and the total stress is the sum of the stresses in each element. It is represented in figure 2.6, where E_∞ is the long term modulus.

So the stress experienced by the system is

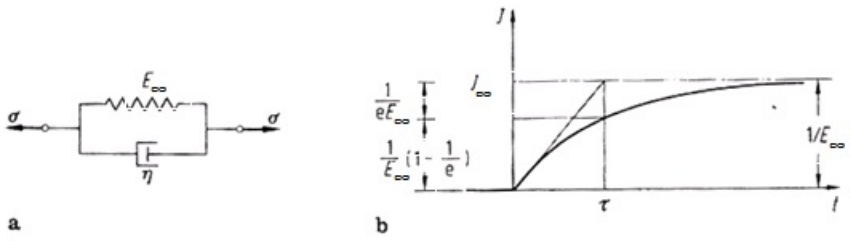

Figure 2.6: Kelvin-Voigt model and its creep function $J(t)$ vs time. [13]

$$\sigma = E_\infty(\epsilon + \tau_c\dot{\epsilon}) \quad , \tag{2.24}$$

with the retardation time $\tau_c = \eta/E_\infty$. The creep response of the Voigt model is, as shown in figure 2.6:

$$J(t) = \frac{1}{E_\infty}(1 - e^{-t/\tau_c}) \quad , \tag{2.25}$$

and the relaxation response is a constant plus a delta function [18].

In conclusion, the strain approaches to a final nonzero value, presenting stress relaxation, which fits to viscoelastic behavior. However, it has rigid behavior at the beginning, with creep compliance $J_{(t=0)} = 0$, so this model is not suitable for modeling viscoelasticity.

The Maxwell model

The Maxwell model consists of a spring and dashpot in series. Because inertia is neglected, the stress is the same in both elements; and the total strain is the sum of the strains. This model is represented in figure 2.7, with E representing this time the instantaneous relaxation moduli E_0.

The stress for this model takes the form

$$\sigma + \tau\dot{\sigma} = \eta\dot{\epsilon} \quad , \tag{2.26}$$

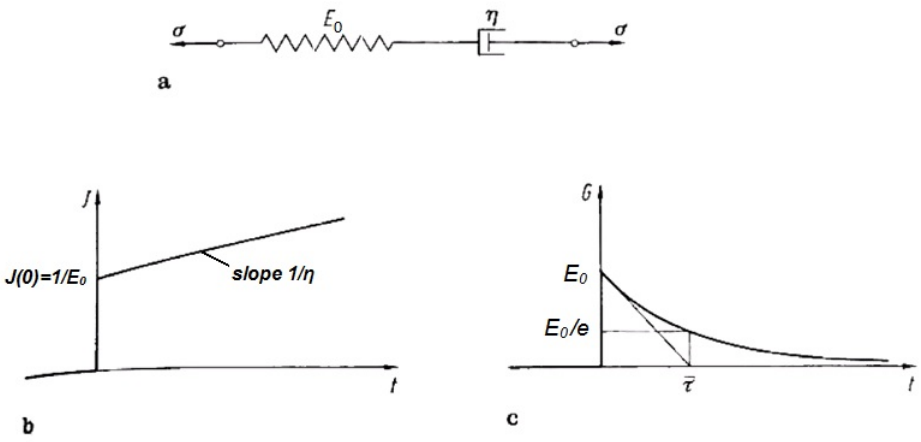

Figure 2.7: Maxwell model with its creep function $J(t)$, and its relaxation function $E(t)$. [13]

with τ as η/E_0. If we input step strain, the relaxation response in terms of the relaxation modulus is found to be, with $\tau = \tau_r$:

$$E(t) = E_0 e^{-t/\tau_r} \quad , \tag{2.27}$$

however, if we input step stress, the creep response is

$$J(t) = \frac{1}{E_0}\frac{t}{\eta} \quad . \tag{2.28}$$

As we can see in the equations above and on figure 2.7, the Maxwell body has a sudden strain increase to the stress change, so it has solid-like behavior in the beginning, but the strain goes to an infinite value in constant stress tests and the stress relaxes to zero, so it has liquid-like final behavior, so it is also unsuitable.

Standard linear solid

There are two different configurations with equivalent results. One possibility would be a series configuration of Hooke's body and Kelvin-Voigt body, and the other would be a parallel configuration of Hooke's body and Maxwell body.

An example of each case is given in figure 2.8. In this case the creep function stands for

$$J(t) = \frac{1}{E_\infty} - \frac{E_1}{E_\infty(E_1 + E_\infty)} e^{-t/\tau_c} \quad , \tag{2.29}$$

and the relaxation function for

$$E(t) = E_\infty + E_1 e^{-t/\tau_r} \quad , \tag{2.30}$$

where $\tau = \tau_r$ and

$$\tau_c = \tau_r \frac{(E_1 + E_\infty)}{E_\infty} \quad . \tag{2.31}$$

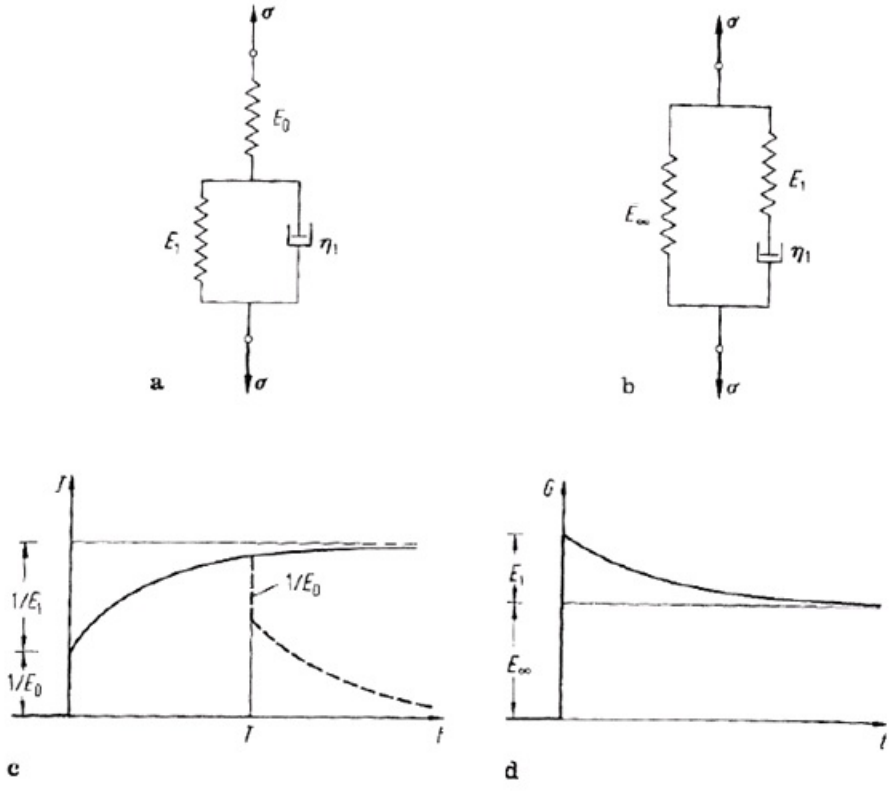

Figure 2.8: Two configurations for standard linear solid model with its creep function $J(t)$, and its relaxation function $E(t)$. [13]

Observe that the retardation time is not equal to the relaxation time; it is larger. In conclusion, this model is suitable to modeling viscoelasticity, as it presents a finite instantaneous elastic moduli $E_0 = E_\infty + E_1$, which relaxes with time to a long term finite elastic modulus E_∞.

This model can be expanded by more Maxwell bodies connected in parallel, as showed in

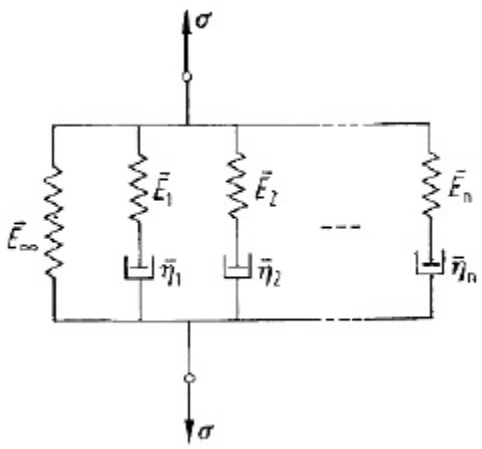

Figure 2.9: Model of complex standard linear solid group. [13]

figure 2.9; the relaxation function consists now in a sum of several exponential functions, which can be developed in terms of Prony series [33].

The group presented in figure 2.9 has an instantaneous elastic modulus and a relaxation function dependent on every parallel element, i.e. Hooke's body and Maxwell's bodies, where each Maxwell body corresponds to a sum element, providing a portion of the temporary stress profile. On the other hand, the long term behavior depends only on the elastic modulus of the Hooke's body E_∞.

Chapter 3

Applied FEM techniques and resources

The present thesis uses ABAQUS Standard version 6.14 from Dassault Systèmes, as this software uses the Finite Element Method or FEM, a contextualization and a short explanation of its main used features are given in this chapter.

3.1 Introduction

The limitations of the human mind are such that it cannot grasp the behavior of its complex surroundings and creations in one operation. In many situations an adequate model is obtained using a finite number of well-defined components. We shall term such problems *discrete*. In others the subdivision is continued indefinitely and the problem can only be defined in terms of differential equations or equivalent statements that imply an infinite number of elements. We shall term such systems *continuous*.

With the advent of digital computers, *discrete* problems can generally be solved readily even if the number of elements is very large. As the capacity of all computers is finite, *continuous* problems can only be solved exactly by mathematical manipulation. Here, the available mathematical techniques usually limit the possibilities to oversimplified situations.

To overcome the intractability of realistic types of continuum problems, various methods of *discretization* have been proposed from time to time by engineers and mathematicians. All involve an *approximation*, a mathematical model, which, hopefully, approaches in the limit the true continuum solution as the number of discrete variables or elements increases.[32]

This *discrete* arrangement of elements is commonly known as mesh, and the finite element procedure uses it to solve the differential equations of the simplified mathematical model. Since the FEM is a numerical procedure, it is necessary to assess the solution accuracy. If the accuracy criteria are not met, the numerical solution has to be repeated with refined solution parameters (such as finer meshes) until a sufficient accuracy is reached.

It is clear that the finite element solution will solve only the selected mathematical model and that all assumptions and approximations in this model will be reflected in the predicted response. Hence the choice of an appropriate mathematical model is crucial and completely determines the insight into the actual physical problem that we can obtain by the analysis. [4] The procedure is illustrated in figure 3.1.

3.2 Periodic Microfield Models

Periodic Microfield Approaches or PMAs aim at approximating the macroscopic and microscopic behavior of inhomogeneous materials by studying model materials that have periodic microstructures. In the context of these thesis, they are used to obtain material data and to perform some tests of reliability of the UMAT.

3.2.1 Basic concepts of unit cell models

Periodic microfield approaches analyze the behavior of infinite (one, two- or three-dimensional) periodic phase arrangements under the action of far field mechanical loads or uniform temperature fields. The most common approach to studying the stress and strain fields in such periodic configurations is based on describing the microgeometry by a periodically repeating unit cell to which the investigations may be limited without loss of information or generality, at least for static analysis.

A *unit cell* is any volume element that can generate a periodic microgeometry. Accordingly, a unit cell may comprise a simple periodic base unit (or part of it), a collective of simple periodic base units, or a phase arrangement of arbitrary geometrical complexity (multi-fiber or multi-particle unit cell) that shows translational periodicity; in the limiting case a unit cell may thus be a representative volume element, which is a subvolume of the whole volume under study

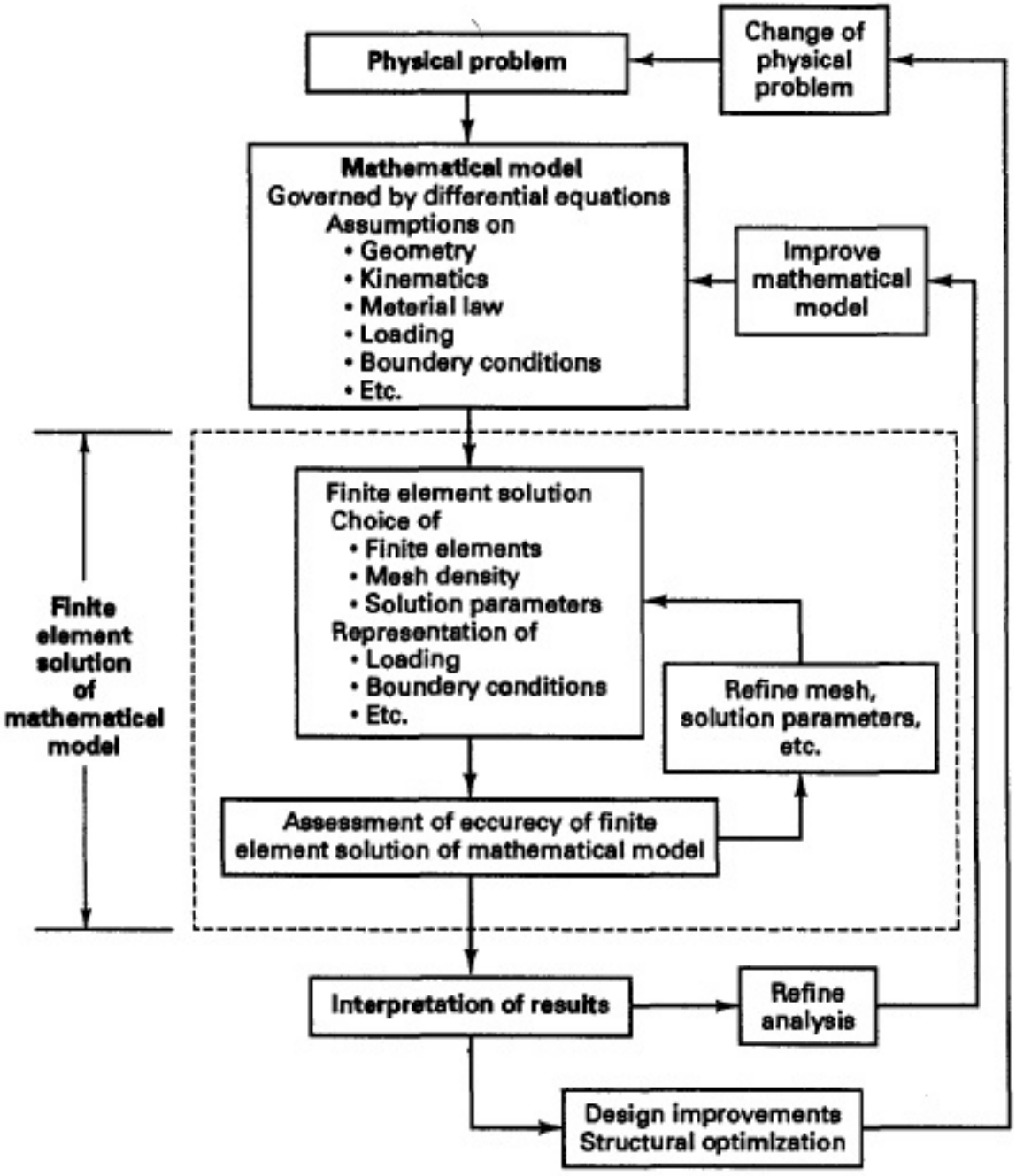

Figure 3.1: The process of finite element analysis. [4]

that is of sufficient size to contain all information necessary for describing the behavior.

The literature on periodic homogenization of inhomogeneous materials is fairly extensive, and well developed mathematical theories are available on scale transitions in periodic structures, compare [21]. For further detail see [6].

3.2.2 Boundary conditions (B.C.s)

Unit cells together with the boundary conditions (B.C.s) prescribed on them must generate valid tilings both of the undeformed geometry and for all deformed states pertinent to a given micromechanical problem. Accordingly, gaps and overlaps between neighboring unit cells as well as nonphysical constraints on their deformations must not be allowed, i.e., the cells must be geometrically compatible. In order to achieve this, the boundary conditions for the unit cells must be specified in such a way that all deformation modes appropriate for the load cases to be studied can be attained. The three major types of boundary conditions used in periodic microfield analysis are periodicity, symmetry and antisymmetry or point symmetry.

In PMA models one of these three types of boundary conditions (or a combination of them) must be used, irrespective of the numerical method employed for solving the equilibrium equations. Generally, for a given periodic phase arrangement unit cells are non-unique, the range of possible shapes being especially wide when point or mirror symmetries are present in the microgeometry (as tends to be the case for regular lattices). As an example, figure 3.2 depicts a (two-dimensional) periodic hexagonal array of circular inhomogeneities (e.g., fibers oriented normally to the plane) and some of the unit cells that can be used to study aspects of the behavior of this phase arrangement. There are considerable differences in the sizes and capabilities of the unit cells shown. [6]

In the following a nomenclature is used in which the faces of two-dimensional quadrilateral unit cells are denoted as N, S, E and W (for North, South, East, and West which are used as in topographical maps), vertices being named according to the adjoining cell faces, compare figures 3.5 and 3.6. The faces of three-dimensional cells of hexahedral shape are, by analogy, referred to as N, S, E, W, B and T (the latter standing for bottom and top), and edges as well as vertices are referred to via the adjoining faces (e.g., SE or SWB), see figure 3.4.

As periodic and symmetry boundary conditions are some of the B.C.s used in the present

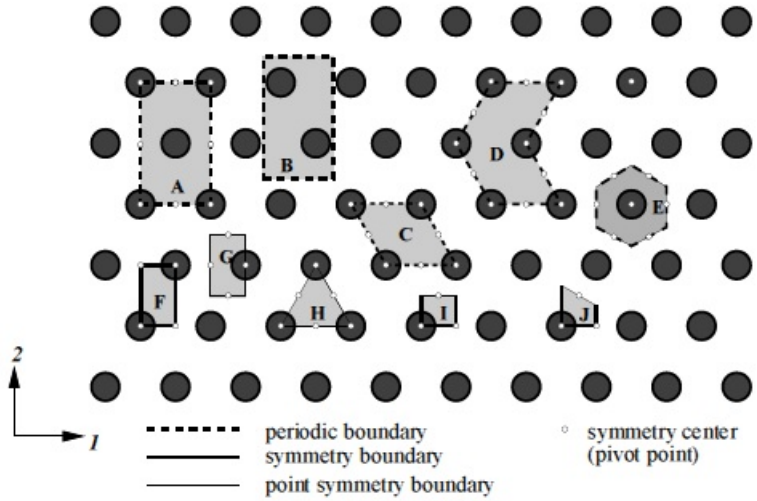

Figure 3.2: Periodic hexagonal array of circular inhomogeneities in a matrix and 10 unit cells that can be used to describe the mechanical responses of this arrangement under loads acting parallel to the coordinate axes. [6]

work, few further details about them will be given.

Periodicity boundary conditions

They are the most general boundary conditions for unit cells in periodic microfield approaches. They can handle any physically valid deformation state of the cell and, consequently, of the material to be modeled. Periodicity boundary conditions make use of translation symmetries of a given geometry; in figure 3.2 cells A to E belong to this group.

In order to describe an N-dimensional phase arrangement with translation periodicity, a suitable unit cell and a set of N linearly independent periodicity vectors $\boldsymbol{p_n}$ are required. These periodicity vectors are neither unique nor do they have to be orthogonal. The surface of any unit cell to be used with periodicity boundary conditions must consist of at least N pairs of faces (or pairs of parts of faces) Γ_k, and the surface elements making up a given pair, k^+ and k^-, must be identical but shifted relative to each other by "shift vectors" $\boldsymbol{c_k}$. Each shift vector, in turn, must be a linear combination of the periodicity vectors, i.e. $\boldsymbol{c_k} = \sum_l c_l^k \boldsymbol{p_l}$, where the c_l^k are integer numbers. In figure 3.3 are represented some examples of possible periodic unit cells, matching pairs of faces (or, in the case of some cells, parts of faces) Γ_k are marked by being drawn in the same line style.

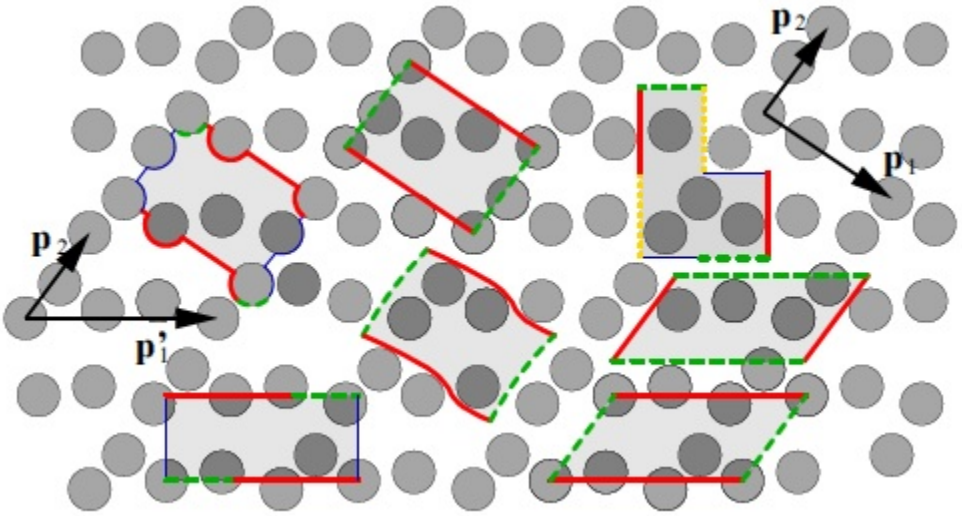

Figure 3.3: Seven different but equivalent periodic minimum-size unit cells for a two-dimensional periodic matrix–inclusion medium with two (slightly) non-orthogonal periodicity vectors $\boldsymbol{p_1}$ and $\boldsymbol{p_2}$ ($\boldsymbol{p_1'}$ and $\boldsymbol{p_2}$ form an alternative pair of periodicity vectors). Paired faces (or parts of faces) Γ_k are marked by identical line styles and regions belonging to one of the cells are highlighted by shading. [6]

Unit cells of simple shape to some extent facilitate the application of periodicity boundary conditions, like in figure 3.4.

Because the unit cells tile the computational space by translation, neighboring cells (and, consequently, the "opposite" faces of a given cell) must fit into each other like the pieces of a jigsaw puzzle in both undeformed and deformed states. For each pair of surface elements, Γ_k , the periodicity boundary conditions for the mechanical problem in the small strain regime look like

$$\boldsymbol{\Delta u_k} = \boldsymbol{u_{k^+}} - \boldsymbol{u_{k^-}} = \boldsymbol{u(s_k + c_k)} - \boldsymbol{u(s_k)} = \langle \epsilon \rangle * \boldsymbol{c_k} \quad , \tag{3.1}$$

where $\boldsymbol{u_{k^-}}$ and $\boldsymbol{u_{k^+}}$ are the displacements at pairs of "homologous" points $\boldsymbol{s_k}$ and $\boldsymbol{s_k} + \boldsymbol{c_k}$ on the surface elements k^- and k^+ (which may, e.g., correspond to faces N and S in figures 3.4 and 3.5, respectively. The vector linking such pairs of points is in a deformed state is $\hat{\boldsymbol{c}}_{\boldsymbol{k}} = \boldsymbol{c_k} + \boldsymbol{\Delta u_k}$. These conditions enforce a "seamless fit" between neighboring unit cells for all possible deformed states.

For numerical analysis the two faces making up a pair Γ_k must be discretized in a compatible

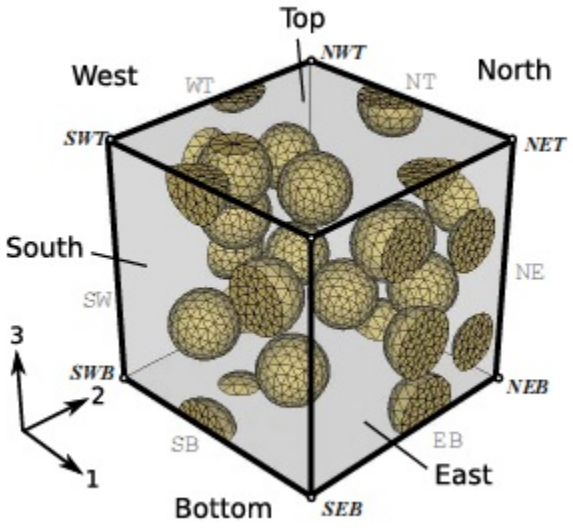

Figure 3.4: Cube-shaped periodic unit cell containing 15 randomly positioned spherical particles of equal size at a volume fraction of $\epsilon^{(i)} = 0.15$. Designators of the six faces (East, West, North, South, Top, Bottom) and of the vertices are given.[24]

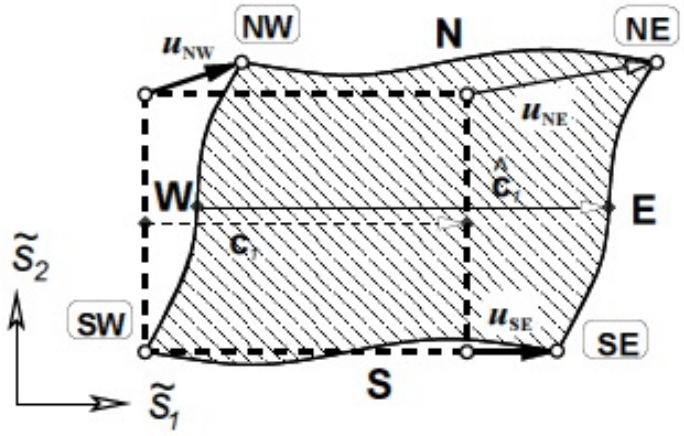

Figure 3.5: Sketch of periodicity boundary conditions as used with an initially rectangular two-dimensional unit cell.[6]

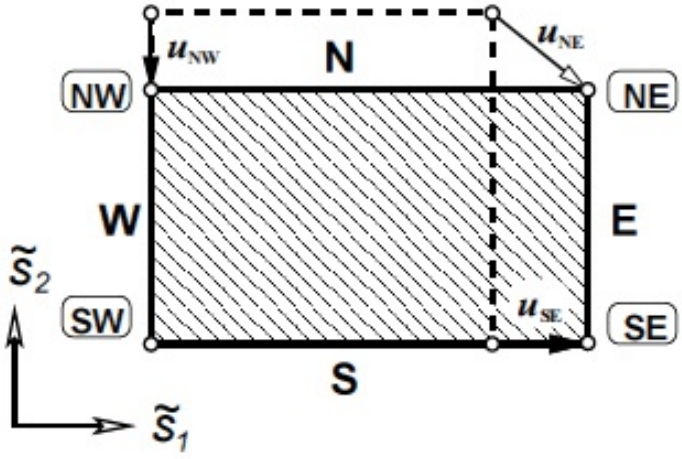

Figure 3.6: Sketch of symmetry boundary conditions as used with a rectangular two-dimensional unit cell.[6]

way, i.e., the nodal points on them must be positioned at equal values of the "face coordinates" s_k. Equations (3.1) then become sets of linear constraints each of which links three nodal displacement DOFs. Equation (3.1) shows that the displacements of the "master nodes", SE and NW, contain the information on the macroscopic strain tensor $\langle\epsilon\rangle$. In addition, the displacements of the master nodes and of faces S and W fully control the displacements of the "slave faces" N and E. [6]

Symmetry boundary conditions

For rectangular and hexahedral unit cells in which the faces of the cell coincide with symmetry planes of the phase arrangement and for which this property is retained for all deformed states that are to be studied, periodicity B.C.s simplify to symmetry (or mirror) boundary conditions. Following the nomenclature of figure 3.6 these B.C.s take the form

$$u_E(\tilde{s}_2) = u_{SE} \qquad v_N(\tilde{s}_1) = v_{NW} \qquad u_W(\tilde{s}_2) = 0 \qquad u_S(\tilde{s}_1) = 0 \quad , \tag{3.2}$$

where u and v stand for the displacement components in 1- and 2-direction, respectively. Equation (3.2) puts constraints on the normal displacement components at the unit cells' surfaces, but leaves the tangential displacements free.

The load cases that can be handled are limited to uniform thermal loads or mechanical loads

that act in directions normal to one or more pairs of faces.

3.2.3 Application of loads and evaluation of fields

Once suitable unit cells have been defined and appropriate B.C.s applied, the volume elements must be subjected to appropriate loads in the form of uniform macroscopic stresses as well as strains, homogeneous temperature excursions, or suitable transformation strains, i.e., the microscopic and macroscopic fields must be linked.

The *method of macroscopic degrees of freedom* consists in applying far field stresses and strains to a given unit cell via concentrated nodal forces or prescribed displacements, respectively, at the master nodes and/or pivot points. The displacements or reaction forces at the master nodes, in turn, can be used to evaluate the macroscopic strains and stresses acting on the composite.

In order to obtain three-dimensional homogenized elastic tensors with the method of macroscopic degrees of freedom, six suitable, linearly independent load cases must be solved for in the most general case.

Chapter 4

Material symmetries and UMAT development

In this chapter the generalized Hooke's law is presented. Some different material symmetries will be dealt too, this material symmetries simplify the problem, as less independent parameters for defining the material behavior are needed. Finally, how via UMAT those material symmetries are implemented will also be detailed.

4.1 Generalized Hooke's Law

In equation (2.1), Hooke's Law is for 1-dimensional cases represented, but it should be generalized, as such an equation does not apply anymore regarding 2D or 3D cases, in which the stress is not a single value anymore, but a second-rank tensor $\boldsymbol{\sigma_{ij}}$:

$$\boldsymbol{\sigma_{ij}} = \begin{pmatrix} \sigma_{11} & \sigma_{12} & \sigma_{13} \\ \sigma_{21} & \sigma_{22} & \sigma_{23} \\ \sigma_{31} & \sigma_{32} & \sigma_{33} \end{pmatrix} \quad . \tag{4.1}$$

Because of its symmetry properties, we can write the stress tensor $\boldsymbol{\sigma_{ij}}$ as

$$\boldsymbol{\sigma_i} = \begin{pmatrix} \sigma_1 \\ \sigma_2 \\ \sigma_3 \\ \sigma_4 \\ \sigma_5 \\ \sigma_6 \end{pmatrix} \quad , \tag{4.2}$$

where $\sigma_1 = \sigma_{11}$, $\sigma_2 = \sigma_{22}$, $\sigma_3 = \sigma_{33}$, $\sigma_4 = \sigma_{12}$, $\sigma_5 = \sigma_{13}$ and $\sigma_6 = \sigma_{23}$. The same procedure can be applied with the strain tensor $\boldsymbol{\epsilon_{ij}}$. In the present work, engineering shear strain is considered, as it is the convention used by Abaqus software. Considering engineering shear strain as

$$\gamma_{ij} = 2\epsilon ij \quad \text{for} \quad i \neq j \quad . \tag{4.3}$$

The resulting stress $\boldsymbol{\sigma_{ij}}$ to an applied strain $\boldsymbol{\epsilon_{ij}}$ is such that each component is linearly related to all the components of the strain [23]. Thus, for example, without considering the symmetry of the strain tensor, σ_{11} would linearly depend on each one of the nine components of ϵ_{ij}. In terms of that, we can write the generalized form of Hooke's Law:

$$\boldsymbol{\sigma_{ij}} = \boldsymbol{E_{ijkl}\epsilon_{kl}} \quad , \tag{4.4}$$

where $\boldsymbol{E_{ijkl}}$ is the *elasticity tensor* and is composed by the *elastic constants* of the material. As $\boldsymbol{\epsilon_{ij}}$ and $\boldsymbol{\sigma_{ij}}$ are in general second order tensors, $\boldsymbol{E_{ijkl}}$ is a fourth order tensor.

If we apply only one component of stress, say σ_{11}, equation (4.4) imply that all the strain components, not just ϵ_{11}, may be different from zero.

Equation (4.4) stands for nine equations, each with nine terms on the right-hand side. So there are 81 E_{ijkl} coefficients. On the other hand, as stated above, strain and stress tensors are symmetric. In consequence, only 36 of the 81 components E_{ijkl} can be independent and we can represent the fourth rank stiffness tensor as a 2 dimensional tensor $\boldsymbol{E_{ij}}$ as follows

$$\boldsymbol{\sigma_i} = \boldsymbol{E_{ij}\epsilon_j} \quad , \tag{4.5}$$

where $\boldsymbol{E_{ij}}$ is also symmetric. Hence, there are at most 21 different components in the elas-

ticity tensor for the most anisotropic case.

4.1.1 Plane theory of elasticity: Plane stress

Many problems in elasticity may be treated satisfactorily by a two-dimensional, or plane theory of elasticity, in consequence, under this assumption the elasticity tensor $\boldsymbol{E_{ij}}$ can be reduced from a (6x6) matrix to a (3x3) matrix, reducing considerably the computational effort. There are two general types of problems involved in this plane analysis, *plane stress* and *plane strain*. This two types are defined by setting down certain restrictions and assumptions on the stress and strain fields.

Plane strain is defined to be a state of strain in which the strain normal to the 1-2 plane, or ϵ_{33}, and the shear strains γ_{23} and γ_{13} are assumed to be zero. This assumption is acceptable if one of the dimensions of the model, say the 3 direction, is very large in comparison with the dimensions of the structure in the other two directions.

On the other hand, plane stress is defined to be a state of stress in which the normal stress, σ_{33} and the shear stresses, σ_{23} and σ_{13} are assumed to be zero. This model is useful to treat essentially plate structures, or those which one dimension is much smaller than the others. As this possibility is implemented by one of the UMATs, it will be further developed.

Under plane stress assumption, and regarding equation (4.5) as a system of six equations, it results that ϵ_5 and ϵ_6 are zero, but also that ϵ_3 is linearly dependent from the remaining strains. So it is possible to write the (6x6) elasticity tensor of equation (4.5) as a (3x3) tensor as follows

$$\boldsymbol{E_{ij}} = \begin{pmatrix} E_{11} - E_{13}\frac{E_{13}}{E_{33}} & E_{12} - E_{13}\frac{E_{23}}{E_{33}} & E_{14} - E_{13}\frac{E_{34}}{E_{33}} \\ E_{12} - E_{23}\frac{E_{13}}{E_{33}} & E_{22} - E_{23}\frac{E_{23}}{E_{33}} & E_{24} - E_{23}\frac{E_{34}}{E_{33}} \\ E_{14} - E_{34}\frac{E_{13}}{E_{33}} & E_{24} - E_{34}\frac{E_{23}}{E_{33}} & E_{44} - E_{34}\frac{E_{34}}{E_{33}} \end{pmatrix} , \tag{4.6}$$

where E_{11}, E_{13} are the terms (11) and (13) of the (6x6) $\boldsymbol{E_{ij}}$ original matrix respectively, and so successively. In case the coordinate system in consideration coincides with the principal material axes of a orthotropic material, the tensor would look like

$$\boldsymbol{E_{ij}} = \begin{pmatrix} E_{11} - E_{13}\frac{E_{13}}{E_{33}} & E_{12} - E_{13}\frac{E_{23}}{E_{33}} & 0 \\ E_{12} - E_{23}\frac{E_{13}}{E_{33}} & E_{22} - E_{23}\frac{E_{23}}{E_{33}} & 0 \\ 0 & 0 & E_{44} \end{pmatrix} \quad . \tag{4.7}$$

4.2 Material symmetries

The presence of symmetry in the material properties reduces still further the number of independent E_{ij} parameters.

All the tensors is this section are referred in the way ABAQUS implements them: in terms of engineering strain γ_{ij}, introduced in equation (4.3).

Orthotropic materials

Some engineering materials, including certain piezoelectric materials, e.g. Rochelle salt [5], or wood, are orthotropic.

By definition, an orthotropic material has at least three orthogonal planes of symmetry. Such materials require nine independent parameters (i.e. elastic constants) in their constitutive matrices [23]. Various sets of these parameters can be given, their choice is not unique.

So its elasticity matrix, found as the inverse of the *compliance matrix* of the material, which is the matrix which linearly relates strains to stresses, looks like [8]

$$\boldsymbol{E_{ij}} = \begin{pmatrix} \frac{1-\nu_{yz}\nu_{zy}}{E_yE_z\Delta_1} & \frac{\nu_{yx}+\nu_{zx}\nu_{yz}}{E_yE_z\Delta_1} & \frac{\nu_{zx}+\nu_{yx}\nu_{zy}}{E_yE_z\Delta_1} & 0 & 0 & 0 \\ \frac{\nu_{xy}+\nu_{xz}\nu_{zy}}{E_zE_x\Delta_1} & \frac{1-\nu_{zx}\nu_{xz}}{E_zE_x\Delta_1} & \frac{\nu_{zy}+\nu_{zx}\nu_{xy}}{E_zE_x\Delta_1} & 0 & 0 & 0 \\ \frac{\nu_{xz}+\nu_{xy}\nu_{yz}}{E_xE_y\Delta_1} & \frac{\nu_{yz}+\nu_{xz}\nu_{yx}}{E_xE_y\Delta_1} & \frac{1-\nu_{xy}\nu_{yx}}{E_xE_y\Delta_1} & 0 & 0 & 0 \\ 0 & 0 & 0 & G_{xy} & 0 & 0 \\ 0 & 0 & 0 & 0 & G_{xz} & 0 \\ 0 & 0 & 0 & 0 & 0 & G_{yz} \end{pmatrix} \quad , \tag{4.8}$$

which is symmetric, where

$$\Delta_1 = \frac{1 - \nu_{xy}\nu_{yx} - \nu_{yz}\nu_{zy} - \nu_{zx}\nu_{xz} - 2\nu_{xy}\nu_{yz}\nu_{zx}}{E_xE_yE_z} \quad , \tag{4.9}$$

with E_x, E_y and E_z the respective Young's Moduli in the x, y and z directions, ν_{ij} the Poisson's ratio in the j direction when a stress or strain is applied on the i direction, and G_{ij} are the shear moduli.

Even though nine independent parameters are needed for its implementation, the terms on the elasticity matrix can be obtained via six material tests, e.g. three tensile and three shear tests, as from the tensile tests we can compute both Young modulus and Poisson's ratio. Depending on which kind of boundary conditions we use, we can obtain each of the material parameters present in the matrix separately, or directly the terms of the stiffness tensor.

Transversally isotropic materials

A special class of orthotropic materials are those that have the same properties in one plane (e.g. the x-y plane) and different properties in the direction normal to this plane (e.g. the z-axis). Such materials are called transverse isotropic, and they are described by five independent elastic constants, instead of nine for orthotropic.

Examples of transversely isotropic materials include some piezoelectric materials (e.g. PZT-4, barium titanate [5]) and fiber-reinforced composites where all fibers are in parallel.

For a transversally isotropic material, with isotropy plane x-y, its stiffness matrix can be easily deduced from the orthotropic material's one, it looks like [8]

$$\boldsymbol{E_{ij}} = \begin{pmatrix} \frac{1-\nu_{pz}\nu_{zp}}{E_p E_z \Delta_2} & \frac{\nu_p+\nu_{zp}\nu_{pz}}{E_p E_z \Delta_2} & \frac{\nu_{zp}+\nu_p\nu_{zp}}{E_p E_z \Delta_2} & 0 & 0 & 0 \\ \frac{\nu_p+\nu_{pz}\nu_{zp}}{E_z E_p \Delta_2} & \frac{1-\nu_{zp}\nu_{pz}}{E_z E_p \Delta_2} & \frac{\nu_{zp}+\nu_{zp}\nu_p}{E_z E_p \Delta_2} & 0 & 0 & 0 \\ \frac{\nu_{pz}+\nu_p\nu_{pz}}{E_p^2 \Delta_2} & \frac{\nu_{zp}+\nu_{pz}^2}{E_p^2 \Delta_2} & \frac{1-\nu_p^2}{E_p^2 \Delta_2} & 0 & 0 & 0 \\ 0 & 0 & 0 & \frac{E_p}{2(1+\nu_p)} & 0 & 0 \\ 0 & 0 & 0 & 0 & G_{xz} & 0 \\ 0 & 0 & 0 & 0 & 0 & G_{xz} \end{pmatrix} , \tag{4.10}$$

with E_p and ν_p respectively the Young's Moduli and the Poisson's Ratio of the considered material in the symmetry x-y plane, and

$$\Delta_2 = \frac{1-\nu_p^2-\nu_{pz}\nu_{zp}-\nu_{zp}\nu_{pz}-2\nu_p\nu_{pz}\nu_{zp}}{E_p^2 E_z} . \tag{4.11}$$

In this case, at least three material tests are needed, e.g. two tensile and one shear test. And once again, depending on which kind of boundary conditions we use, we can obtain each of the material parameters present in the matrix separately, or directly the terms of the stiffness tensor.

Cubic material symmetry

Cubic material symmetry can be regarded as the one with the lowest grade of anisotropy. The number of independent elastic material parameters is three, e.g. the bulk modulus, K, and the shear modulus, G and M, being G in this case the shear modulus related to normal loads that involve no volume change, or the shear modulus in the 45º direction. This is a convenient choice for treating the present problem of viscoelasticity [27].

The elasticity matrix for cubic symmetry can also be specified in terms of equation 4.8, but another representation is shown for convenience as follows

$$\boldsymbol{E_{ij}} = \begin{pmatrix} K+\frac{4}{3}G & K-\frac{2}{3}G & K-\frac{2}{3}G & 0 & 0 & 0 \\ K-\frac{2}{3}G & K+\frac{4}{3}G & K-\frac{2}{3}G & 0 & 0 & 0 \\ K-\frac{2}{3}G & K-\frac{2}{3}G & K+\frac{4}{3}G & 0 & 0 & 0 \\ 0 & 0 & 0 & M & 0 & 0 \\ 0 & 0 & 0 & 0 & M & 0 \\ 0 & 0 & 0 & 0 & 0 & M \end{pmatrix} . \tag{4.12}$$

In this case, at least two different material tests are needed, e.g. one tensile test, from where E and ν are extracted, and one load case which fulfills $\sigma_{11} = -\sigma_{22}$, $\sigma_{33} = 0$, which represents a normal load case with no volume change, or a 45º shear test.

Isotropy

An isotropic material has the same properties in every direction, so it shows responses which are independent of the loading direction. Isotropic materials have an infinite number of planes of symmetry. In consequence, if the reference axes are transformed by the operation of a centre of symmetry, the components of $\boldsymbol{E_{ijkl}}$ remain unaltered [23].

Accordingly, the stiffness matrix for isotropic materials is the same as for cubic anisotropic materials, i.e. equation (4.12), but with $G = M$.

One material test is enough to obtain the two independent parameters that are needed for constructing the isotropic stiffness matrix, e.g. a tensile test.

4.3 UMAT development procedure

A UMAT is a subroutine that, implementing a material constitutive model, allows to set a User-defined mechanical material behavior in Abaqus.

To see the different components of the subroutine interface, see appendix A.

In the case of the present thesis, as a linear viscoelastic material is studied under steady state dynamics conditions, the material input data is frequency dependent. This material input data will be the results obtained from different simulations that depend, as seen in the previous section of this chapter, on the material symmetries.

In consequence, the UMAT will have as input different material properties at each frequency that was computed in the material data extraction. If the frequency under study is not one of those in the input data, but in between, linear interpolation of the input material data will be applied. On the other hand, in case such frequency is over the maximum frequency in the input data or below the minimum one, the upper and the lower frequency material data will be considered in the UMAT calculations correspondingly.

After the modulus and its loss angle interpolation, in case it was necessary, of the complex input material properties, such input data is converted in terms of its real and imaginary parts. Afterwards, the storage and the loss material elasticity matrices are computed for the corresponding frequency under study and passed into Abaqus.

To see the input format of the developed UMATs see appendix B.

Chapter 5

UMAT intense testing and application

In this chapter some simulations will be carried out to test the UMAT's accuracy and limitations. Three UMATs are programmed, one specific for cubic anisotropy which can also deal with isotropy; another one, much more complex, to deal with orthotropy, so it can also be applied for transversal isotropy, cubic anisotropy and isotropy; and finally one with the same structure as the orthotropic UMAT, but aimed at dealing with plane stress simulations.

5.1 Cubic UMAT

The material input data extraction, the cubic UMAT intense testing and a finite model application are developed in the present section.

5.1.1 Material input data extraction

The material input data is obtained from the (1x1x1) mm unit cell in figure 5.1 with periodic boundary conditions used in previous works [27]. This way, a regular periodic microstructure can be modeled without imposing any over or under constraints. Macroscopic loading and reading of the unit cell's response is treated via master nodes as explained in section 3.2.3. This way the material behavior is predicted under uniform far field loads without any influence of gradients, free faces, and load introduction.

The unit cell has a relative density of 0.1017. The strut material is a polymer which can be processed by rapid prototyping [29]. For the present study it is taken to be isotropic linear vis-

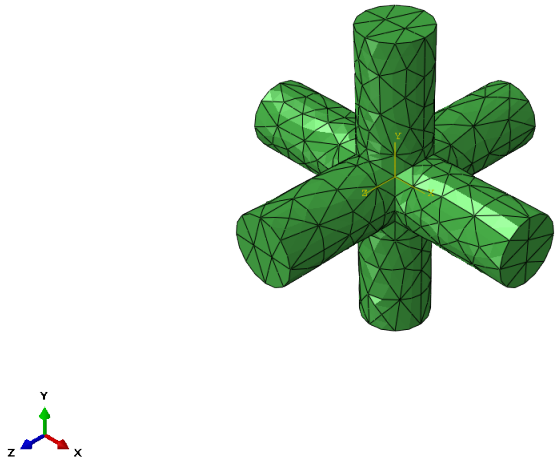

Figure 5.1: Cubic unit cell used for material input data extraction.[27]

coelastic, with the long term elastic Young's modulus, $E_\infty = 118$ [MPa], and Poisson number, $\mu = 0.4$. The relaxation behavior is given in terms of one Prony term in shear with a characteristic time, $\tau^G = 3$ [s], and relative relaxation shear modulus, $g = 0.791$. Such viscoelastic behaviour yielded a maximum loss angle of $\delta = 36.25$ž. The bulk modulus is considered to not show relaxation, i.e. the relative relaxation bulk modulus, $k = 0$. [27]

Volumetric compression tests have been applied at different frequencies in order to get input data of the complex bulk modulus K^* and its loss angle, δ_K, shear tests in the x-z plane for the complex shear modulus M^* and its loss angle, δ_M, and 45º shear tests applying the load case already explained in section 4.2, $\sigma_{11} = -\sigma_{22}$, $\sigma_{33} = 0$ for the input data related to the complex shear modulus G^* and its loss angle, δ_G.

The resulting input data are presented in table 5.1 and graphically represented in figures 5.2 and 5.3.

Table 5.1: Homogenized cubic material data by unit cell simulations.

f [Hz]	K [MPa]	δ_K[°]	G [MPa]	δ_G[°]	M [MPa]	δ_M[°]
10^{-5}	1.93845	0.03653	2.32335	0.03840	0.12920	0.03654
$5.0\cdot10^{-5}$	1.93847	0.20091	2.32338	0.21121	0.12920	0.20094
10^{-4}	1.93852	0.36529	2.32344	0.38400	0.12921	0.36534
$2.5\cdot10^{-4}$	1.93890	0.91304	2.32390	0.95982	0.12923	0.91316
$5.0\cdot10^{-4}$	1.94025	1.82481	2.32555	1.91836	0.12932	1.82507
$7.5\cdot10^{-4}$	1.94249	2.73403	2.32830	2.87433	0.12947	2.73445
10^{-3}	1.94563	3.63945	2.33214	3.82648	0.12968	3.64006
$1.25\cdot10^{-3}$	1.94965	4.53984	2.33706	4.77356	0.12994	4.54070
$2.5\cdot10^{-3}$	1.98274	8.92591	2.37757	9.39215	0.13213	8.92909
$3.75\cdot10^{-3}$	2.03622	13.0264	2.44316	13.7228	0.13567	13.0347
$5.0\cdot10^{-3}$	2.10790	16.7467	2.53126	17.6697	0.14041	16.7635
$6.25\cdot10^{-3}$	2.19514	20.0332	2.63879	21.1782	0.14618	20.0627
$7.5\cdot10^{-3}$	2.29518	22.8695	2.76254	24.2308	0.15280	22.9159
$8.75\cdot10^{-3}$	2.40532	25.2672	2.89933	26.8382	0.16009	25.3344
10^{-2}	2.52307	27.2558	3.04628	29.0291	0.16788	27.3474
$2.0\cdot10^{-2}$	3.53355	33.1880	4.34386	36.2466	0.23498	33.5452
$3.0\cdot10^{-2}$	4.38184	31.3902	5.50125	35.1184	0.29196	32.0082
$4.0\cdot10^{-2}$	4.98961	28.0173	6.38417	31.9547	0.33356	28.8124
$5.0\cdot10^{-2}$	5.40849	24.7221	7.02629	28.6058	0.36284	25.6104
$6.0\cdot10^{-2}$	5.69801	21.8758	7.48933	25.5815	0.38349	22.7972
$7.0\cdot10^{-2}$	5.90186	19.4983	7.82610	22.9791	0.39829	20.4155
$8.0\cdot10^{-2}$	6.04880	17.5234	8.07486	20.7713	0.40911	18.4159
$9.0\cdot10^{-2}$	6.15724	15.8755	8.26194	18.9004	0.41720	16.7329
10^{-1}	6.23909	14.4892	8.40519	17.3079	0.42336	15.3071
$1.25\cdot10^{-1}$	6.37236	11.8505	8.64241	14.2350	0.43352	12.5696

Continued on next page

Table 5.1 – *Continued from previous page*

f [Hz]	K [MPa]	δ_K[º]	G [MPa]	δ_G[º]	M [MPa]	δ_M[º]
$2.5 \cdot 10^{-1}$	6.56633	6.11072	8.99707	7.40206	0.44861	6.52288
$3.75 \cdot 10^{-1}$	6.60453	4.09788	9.06829	4.97224	0.45163	4.38012
$5.0 \cdot 10^{-1}$	6.61808	3.07980	9.09367	3.73918	0.45271	3.29350
$6.25 \cdot 10^{-1}$	6.62438	2.46621	9.10550	2.99507	0.45321	2.63793
$7.5 \cdot 10^{-1}$	6.62781	2.05625	9.11194	2.49758	0.45348	2.19970
$8.75 \cdot 10^{-1}$	6.62989	1.76306	9.11584	2.14166	0.45364	1.88619
1.0	6.63123	1.54299	9.11837	1.87445	0.45375	1.65084
2.5	6.63493	0.61755	9.12532	0.75033	0.45405	0.66080
5.0	6.63546	0.30880	9.12632	0.37520	0.45409	0.33043
7.5	6.63556	0.20587	9.12650	0.25014	0.45409	0.22029
10.0	6.63559	0.15440	9.12656	0.18761	0.45409	0.16522
50.0	6.63554	0.03088	9.12649	0.03752	0.45383	0.03306
100.0	6.63526	0.01544	9.12603	0.01876	0.45300	0.01656

In figure 5.3 we can appreciate the variation in the loss angle with the frequency. which takes the pattern introduced and developed in section 2.2.2. Furthermore it is visible in figure 5.2 the variation of the different considered moduli with frequency, which, in the frequency range of high loss angle, show a noticeable increment in their module to become at high frequencies again stabilized, but to a higher value. The first natural frequency of the unit cell appears approximately between 350 and 400 [Hz], depending on the load case, and the successive eigenfrequencies are close to each other so the pattern of these graphics changes over such frequency.

Considering that for a isotropic material, M and G would take the same value, this results show that the present cubic, porous material has very low resistance when M is triggered, as its M shear modulus is clearly lower as its G shear modulus.

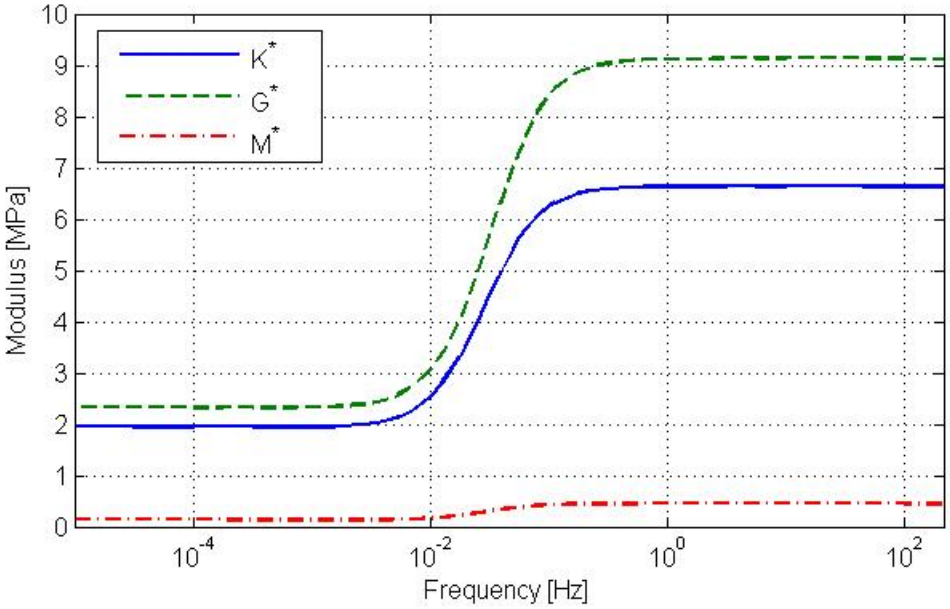

Figure 5.2: Cubic modulus input data in graphical form.

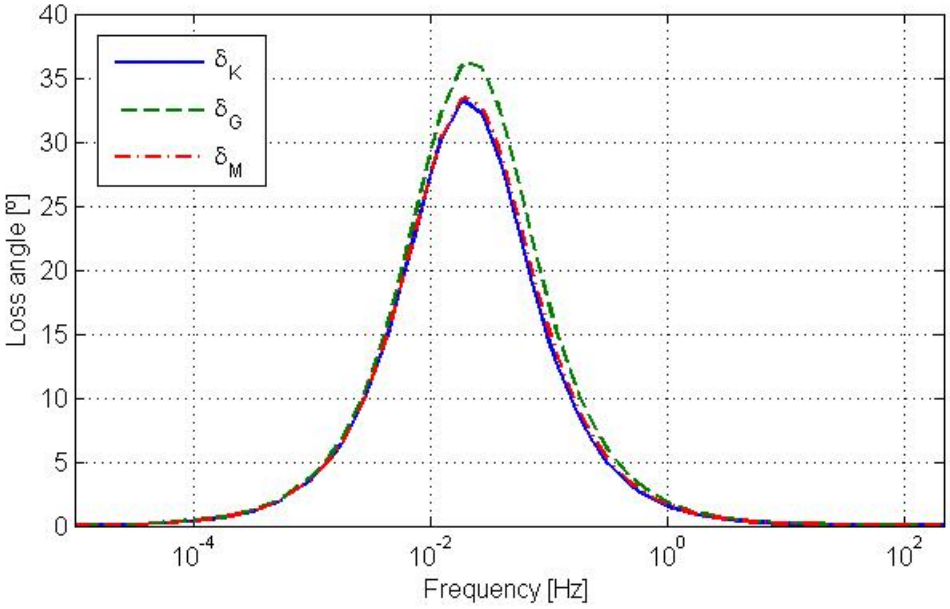

Figure 5.3: Cubic loss angle input data in graphical form.

5.1.2 UMAT intense testing

With the material input data on table 5.1 the cubic UMAT has been intensively tested. The procedure consists in the application of different load cases at different frequencies. The boundary conditions applied to the master nodes in each simulation are represented in table 5.2. Such simulations have been applied to both unit cells, the inhomogeneous cubic unit cell of figure 5.1 with isotropic material data, and a single element with the homogeneized cubic material data of table 5.1, applied through the UMAT subroutine and with periodic boundary conditions.

Table 5.2: Cubic UMAT intense testing load cases. Master nodes' displacement boundary conditions.

		M_0	M_x	M_y	M_z
test 1	d_x [mm]	0	-1	0	0
	d_y [mm]	0	0	0	0
	d_z [mm]	0	0	0	0
test 2	d_x [mm]	0	0.5	0	0
	d_y [mm]	0	0	-	-
	d_z [mm]	0	0.86603	0	-
test 3	d_x [mm]	0	-	-	0.5
	d_y [mm]	0	-	-	0.5
	d_z [mm]	0	0	0	-0.5
test 4	d_x [mm]	0	0	0	-
	d_y [mm]	0	0.5	0	-
	d_z [mm]	0	0	0.5	-
test 5	d_x [mm]	0	0	-	0
	d_y [mm]	0	0.5	0	0
	d_z [mm]	0	0	0	0.5

In the ideal case, each simulation results would coincide correspondingly. This ideal case is actually impossible to achieve because of numerical precision in Abaqus calculations and the number of significant figures chosen for the material input data. Furthermore, if the frequency under study does not coincide with a input data frequency, another error has to be considered, because as presented in section 4.3, a linear interpolation is carried out for the calculations. In conclusion, the more input frequencies used, the more precise the UMAT predictions will be, but some computational errors will always be present.

Table 5.3: Cubic UMAT intense testing average and maximum resulting error in the reference node M_0 main reaction force, RF, and its loss angle, δ calculations.

		average error	maximum error
test 1	RF_1	0.0446%	0.1271%
	δ_1	0.1089%	0.2562%
test 2	RF_1	0.0487%	0.1110%
	δ_1	0.1135%	0.2635%
test 3	RF_3	0.0563%	0.1626%
	δ_3	0.1107%	0.2577%
test 4	RF_1	0.1920%	0.2641%
	δ_1	0.1287%	0.2954%
test 5	RF_3	0.0555%	0.1560%
	δ_3	0.1099%	0.2511%

The comparison of the results given from both models is provided in table 5.3. This comparison is carried out in the $10^{-4} - 10^{0}$ [Hz] frequency range, as it is the range with closest input data. Table 5.3 shows a good prediction from the UMAT, with an error below 1%. Despite that good general precision, if we perform calculations in a frequency range with less input data, the calculations yield higher errors, this is due to the interpolation errors and would be easily

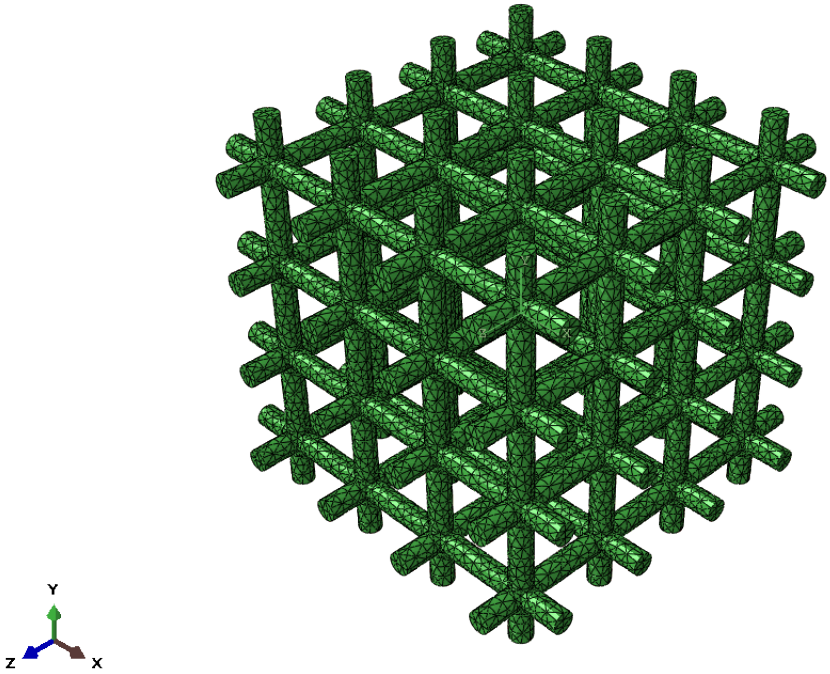

Figure 5.4: Finite model of cubic material in the [001] direction.

solved adding new material input data in the range of frequencies where the calculations will take place.

5.1.3 Finite medium application

The UMAT has been applied to different models of finite size to simulate the effects of load introduction, free faces, and (possibly) open cut base cells. The finite models are four cubic samples which consist in arrays of cells as the one in figure 5.1 with different orientations. These finite models have been previously used in [27].

For every orientation a (virtual) cubic sample of size (8x8x8) mm is investigated, but as for each material orientation different symmetries are present, it is possible to reduce the size of the simulated models. Therefore, smaller finite samples have been simulated. In the case of the [001] and [110] orientations in figures 5.4 and 5.5 respectively, a (4x4x4) mm model is enough, as it is possible to apply symmetry boundary conditions in the xy, xz and yz planes. On the other hand, for the [111] and [120] orientations in figures 5.6 and 5.7 respectively, a (4x8x8) mm model

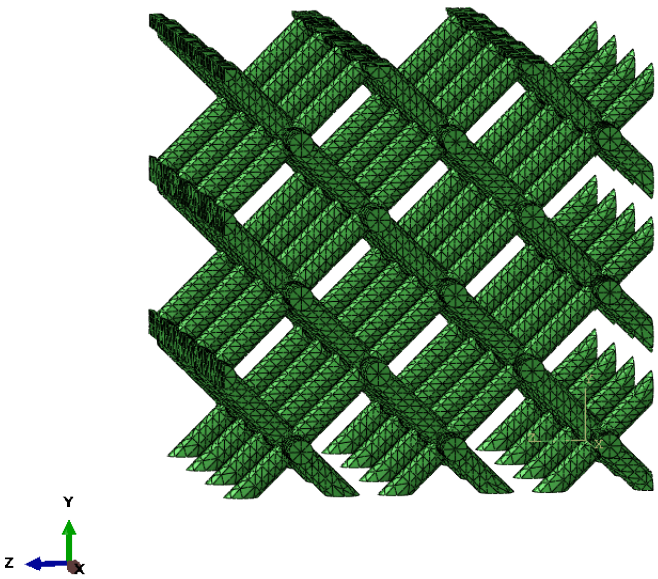

Figure 5.5: Finite model of cubic material in the [110] direction.

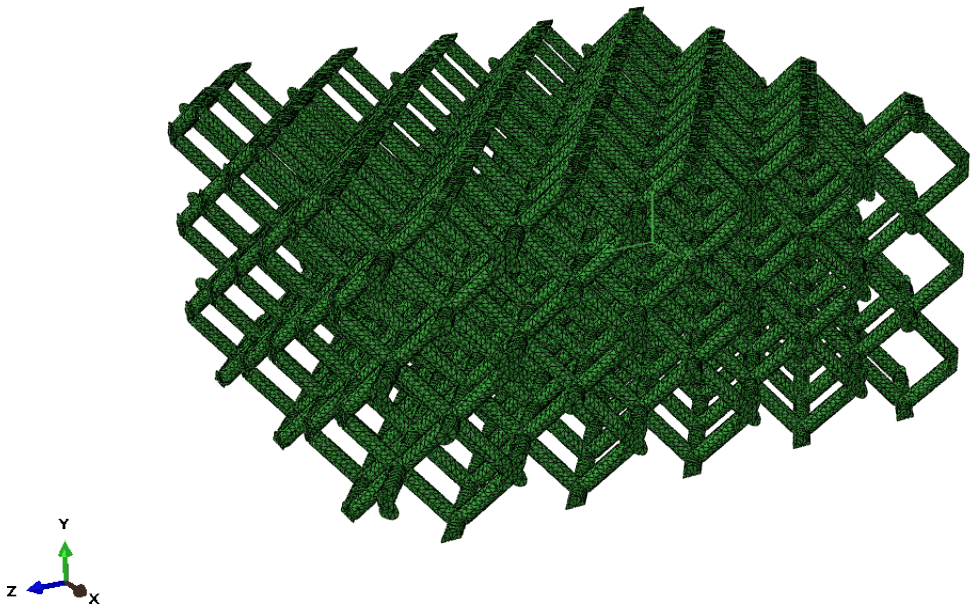

Figure 5.6: Finite model of cubic material in the [111] direction.

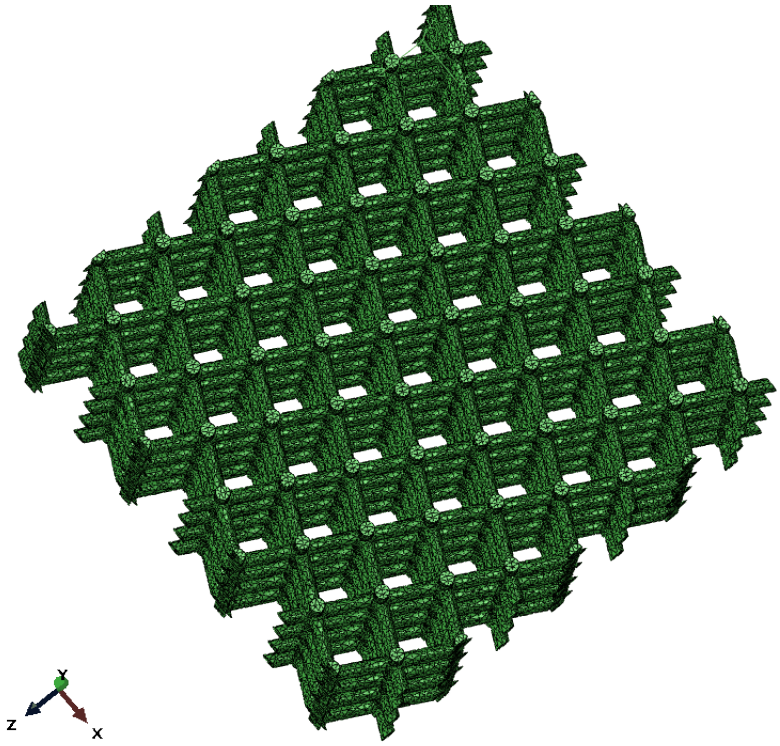

Figure 5.7: Finite model of cubic material in the [120] direction.

is needed, as such orientations have not the previous symmetry properties, so just the symmetry in the xy plane is considered.

Finite models of the same dimensions and boundary conditions, but with homogenized material have been built for the application of the cubic UMAT in order to compare the results given by both finite samples for each material orientation.

Loading conditions are of the type of “uniaxial stress” in the z-direction. The faces with load introduction are thought as having rather massive plates attached to the struts. In addition, all displacement degrees of freedom at the bottom of the structure are locked. At the top face all displacements in loading direction are equal, and the lateral displacements are locked [27].

Table 5.4: Finite models with different material orientations simulation and comparison to the correspondent UMAT results. Reaction force in the stress direction, RF_3, and its loss angle, δ_3.

		frequency [Hz]					
		0.001	0.00373	0.0518	0.193	2.68	10
001	RF_3 [N]	5.028	5.262	14.920	18.390	18.790	18.790
	$RF_{3.UMAT}$ [N]	5.004	5.243	14.790	18.360	18.770	18.760
	δ_3 [º]	3.761	13.410	26.760	8.959	0.659	0.177
	$\delta_{3.UMAT}$ [º]	3.771	13.410	26.940	9.109	0.711	0.177
110	RF_3 [N]	1.034	1.081	3.007	3.677	3.754	3.751
	$RF_{3.UMAT}$ [N]	0.970	1.015	2.776	3.405	3.475	3.438
	δ_3 [º]	3.712	13.230	26.000	8.687	0.639	0.174
	$\delta_{3.UMAT}$ [º]	3.689	13.110	25.770	8.685	0.678	0.171
111	RF_3 [N]	0.506	0.529	1.438	1.751	1.786	1.775
	$RF_{3.UMAT}$ [N]	0.561	0.587	1.584	1.933	1.967	1.874
	δ_3 [º]	3.642	12.980	25.410	8.507	0.626	0.169
	$\delta_{3.UMAT}$ [º]	3.653	12.980	25.270	8.506	0.666	0.174
120	RF_3 [N]	2.201	2.303	6.481	7.972	8.144	8.136
	$RF_{3.UMAT}$ [N]	2.315	2.425	6.779	8.383	8.564	8.478
	δ_3 [º]	3.738	13.320	26.530	8.894	0.654	0.176
	$\delta_{3.UMAT}$ [º]	3.747	13.320	26.600	8.986	0.702	0.177

As we can see in the result table 5.4, the UMAT predictions are quite acceptable, specially in the loss angle calculations, where generally the error is almost zero. The errors are mainly due to the reasons presented above, and the major error in the [111] material orientation might be due to the finite model symmetry consideration, because it is not clear if in this orientation this symmetry actually exists.

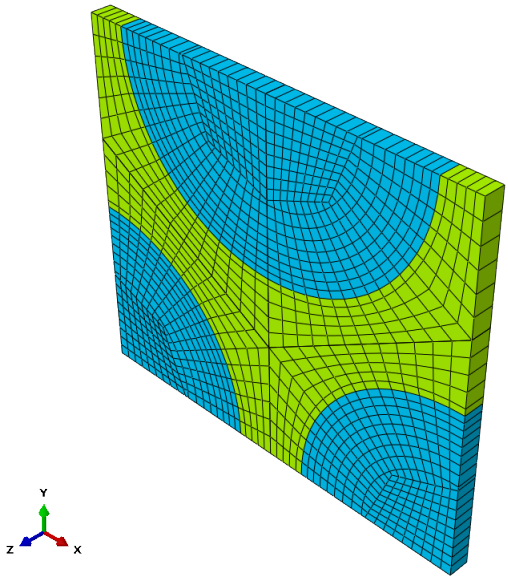

Figure 5.8: Transversal isotropy unit cell. [25]

The complexity of the model and mesh is clearly lower in case of the homogeneous finite sample with the cubic UMAT application, so the preprocessing time is drastically reduced. Furthermore, the reduction in the calculation time is considerably important, e.g. in the finite model with [001] material orientation calculation, the reduction of computation time is 78.57%, and in case of the [111] material orientation, it reaches the 94.39%. In conclusion, the UMAT application has a substantial improvement in computational efficiency with precision costs generally assumable.

5.2 Orthotropic UMAT

In the present section the transversal isotropic material input data extraction and the orthotropic UMAT intense testing with such input data are discussed.

5.2.1 Material input data extraction

In this case the material input data is obtained from the (2x1.73205x0.1) mm unit cell in figure 5.8, developed in [25]. This unit cell yields transversally isotropic material data. The loading and reading of the unit cell's behaviour is the same as the applied in the cubic symmetry case.

The unit cell models a transversally isotropic material composed of matrix and fibers. In the present case, the matrix is considered as the polymer used in the cubic case 5.1.1. On the other hand, the fiber material has a much lower long term elastic modulus, $E = 0.0118$ [MPa], four orders of magnitude lower than the matrix material, and a Poisson number, $\nu = 0.4$, no viscoelastic properties are considered in the fiber material. Such low stiffness fibers behave like voids, so the material can be thought as a transversally isotropic cellular material.

Even though with three would be enough, in order to get the material input data six simulations have been carried out at different frequencies. The reason is with six simulations we can get directly from the Abaqus output each different complex modulus and its phase angle of the elasticity matrix with no need of further calculations. This is convenient as the calculations in the unit cell are not very expensive in terms of computation time. Three confined compression tests in the x-direction with different boundary conditions, one for each, the (11), (12) and (13) terms (the x displacements in order to get directly the values of the tensor as Abaqus output have different magnitudes, as the normal surface for each term is different in the unit cell), one confined compression test in the z-direction for the (33) term, and two shear tests, one in the xy plane for the (44) term and the other in the xz plane for the (55) term. For the input in the orthotropic UMAT, terms (22), (23) and (66) should be also included as input. On the other hand, as the material is transversally isotropic, see section 4.2, terms (11) and (22), (13) and (23), (55) and (66) are equal, so simulations to get such terms are not necessary.

Table 5.5 shows the resulting input data from such simulations. The first eigenfrequency of the system is now approximately between 0.4 and 0.55 [Hz], so the maximum frequency considered for the input material data is 0.375 [Hz]. The material input data is also represented in figures 5.9 and 5.10.

Table 5.5: Homogenized transversal isotropic material data by unit cell simulations.

f [Hz]	**11** [MPa]	δ_{11}[°]	**12** [MPa]	δ_{12}[°]	**13** [MPa]	δ_{13}[°]	**33** [MPa]	δ_{33}[°]	**44** [MPa]	δ_{44}[°]	**55** [MPa]	δ_{55}[°]
10^{-5}	26.870	0.032	14.900	0.030	16.706	0.022	60.570	0.032	5.985	0.035	10.486	0.041
$5.0 \cdot 10^{-5}$	26.870	0.177	14.900	0.163	16.706	0.120	60.571	0.178	5.985	0.195	10.486	0.225
10^{-4}	26.871	0.322	14.900	0.297	16.706	0.218	60.573	0.324	5.985	0.354	10.487	0.409
$2.5 \cdot 10^{-4}$	26.876	0.806	14.903	0.742	16.709	0.545	60.583	0.811	5.987	0.886	10.489	1.021
$5.0 \cdot 10^{-4}$	26.893	1.611	14.912	1.483	16.719	1.088	60.622	1.620	5.991	1.770	10.496	2.041
$7.5 \cdot 10^{-4}$	26.922	2.413	14.927	2.221	16.735	1.630	60.686	2.427	5.997	2.652	10.509	3.059
10^{-3}	26.961	3.211	14.948	2.956	16.758	2.167	60.776	3.231	6.007	3.530	10.527	4.072
$1.25 \cdot 10^{-3}$	27.013	4.005	14.975	3.686	16.786	2.701	60.891	4.029	6.019	4.403	10.550	5.080
$2.5 \cdot 10^{-3}$	27.432	7.864	15.198	7.229	17.023	5.259	61.836	7.913	6.118	8.654	10.737	10.004
$3.75 \cdot 10^{-3}$	28.107	11.453	15.555	10.507	17.400	7.555	63.356	11.526	6.278	12.626	11.041	14.638
$5.0 \cdot 10^{-3}$	29.004	14.684	16.027	13.436	17.897	9.504	65.377	14.782	6.493	16.224	11.451	18.883
$6.25 \cdot 10^{-3}$	30.086	17.508	16.594	15.969	18.487	11.063	67.813	17.633	6.753	19.398	11.953	22.684
$7.5 \cdot 10^{-3}$	31.312	19.915	17.232	18.099	19.143	12.222	70.576	20.067	7.050	22.134	12.533	26.022
$8.75 \cdot 10^{-3}$	32.645	21.919	17.920	19.842	19.841	13.001	73.578	22.100	7.376	24.443	13.177	28.908
10^{-2}	34.050	23.553	18.638	21.231	20.557	13.435	76.743	23.765	7.723	26.356	13.873	31.368
$2.0 \cdot 10^{-2}$	45.320	28.054	24.136	24.425	25.357	9.447	102.244	28.543	10.643	32.171	20.225	40.349
$3.0 \cdot 10^{-2}$	53.988	26.549	28.013	22.552	27.336	1.672	122.192	27.283	13.058	30.839	26.307	40.250
$4.0 \cdot 10^{-2}$	60.063	24.028	30.566	20.137	27.357	5.087	136.525	24.904	14.819	28.044	31.308	37.526

Continued on next page

Table 5.5 – *Continued from previous page*

f [Hz]	**11** [MPa]	δ_{11}[º]	**12** [MPa]	δ_{12}[º]	**13** [MPa]	δ_{13}[º]	**33** [MPa]	δ_{33}[º]	**44** [MPa]	δ_{44}[º]	**55** [MPa]	δ_{55}[º]
$5.0 \cdot 10^{-2}$	64.348	21.576	32.312	17.960	26.466	10.178	146.876	22.502	16.080	25.211	35.192	34.239
$6.0 \cdot 10^{-2}$	67.427	19.408	33.551	16.100	25.256	13.810	154.459	20.328	16.990	22.677	38.144	31.071
$7.0 \cdot 10^{-2}$	69.680	17.543	34.458	14.526	24.007	16.310	160.098	18.427	17.653	20.490	40.378	28.226
$8.0 \cdot 10^{-2}$	71.355	15.949	35.136	13.192	22.839	17.963	164.354	16.785	18.143	18.623	42.074	25.740
$9.0 \cdot 10^{-2}$	72.619	14.585	35.653	12.055	21.794	18.995	167.618	15.369	18.509	17.028	43.372	23.586
10^{-1}	73.586	13.415	36.055	11.080	20.880	19.575	170.157	14.145	18.784	15.662	44.375	21.723
$1.25 \cdot 10^{-1}$	75.156	11.128	36.734	9.176	19.096	19.794	174.449	11.738	19.215	13.002	46.025	18.059
$2.5 \cdot 10^{-1}$	76.677	5.941	37.827	4.825	15.539	14.759	181.094	6.194	19.359	7.054	47.745	9.716
$3.75 \cdot 10^{-1}$	75.308	4.112	38.134	3.242	14.631	10.805	182.460	4.174	18.405	5.062	46.546	6.799

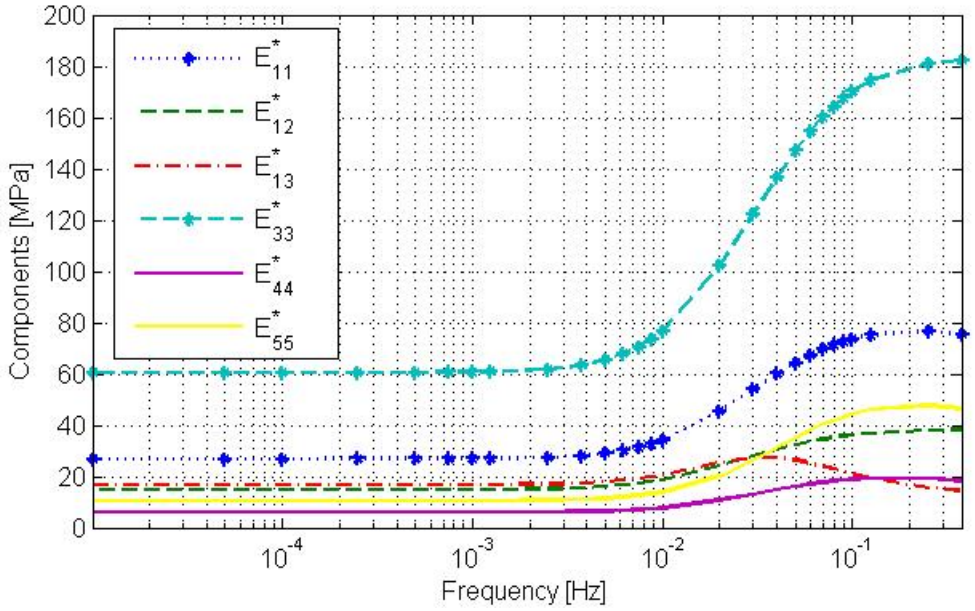

Figure 5.9: Transversally isotropic elasticity matrix components input data in graphical form.

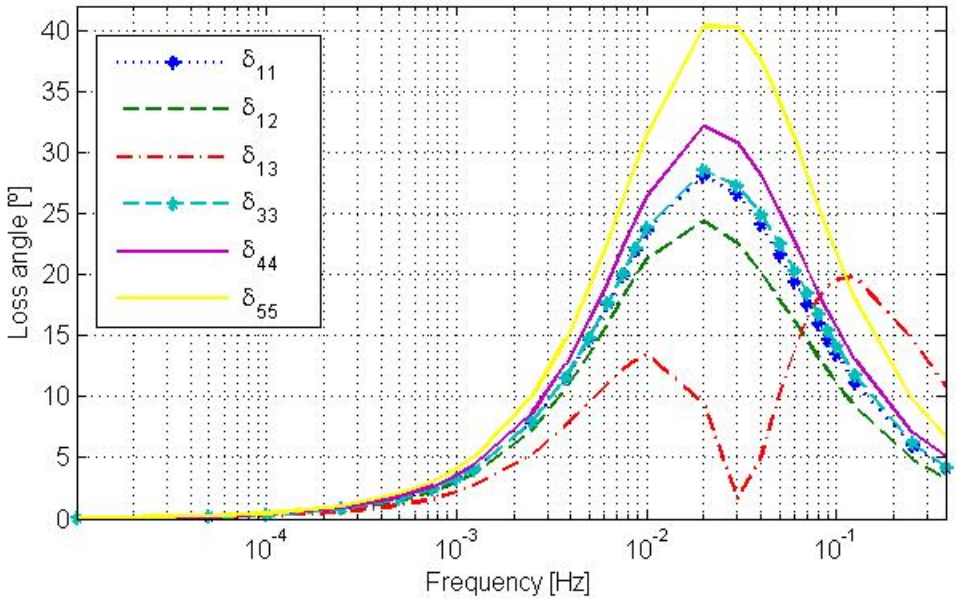

Figure 5.10: Transversally isotropic loss angle input data in graphical form.

The strange results obtained from the unit cell in term (13) might be caused by the fact that the master nodes are placed in the center of the fibers, which in this case act as voids, so the stress transmission might not be as accurate as desired. The effects of this inaccuracy in the

input data will be reflected in the intense testing error results.

5.2.2 UMAT intense testing

The same procedure as with the cubic UMAT has been carried out with the orthotropic UMAT. But in this case, with the boundary conditions of table 5.6, applied to unit cell in figure 5.8 and a single element unit cell with the homogenized transversally isotropic material data of table 5.5, applied though the orthotropic UMAT and with periodic boundary conditions.

Table 5.6: Orthotropic UMAT intense testing load cases. Master nodes' displacement boundary conditions.

		M_0	M_x	M_y	M_z
test 1	d_x [mm]	0	1	0	0
	d_y [mm]	0	0	-	0
	d_z [mm]	0	0	0	-
test 2	d_x [mm]	0	0	0	0
	d_y [mm]	0	1	0	0
	d_z [mm]	0	0	1	0
test 3	d_x [mm]	0	1	0	0
	d_y [mm]	0	0	-	0
	d_z [mm]	0	0	0	0.1
test 4	d_x [mm]	0	0	-	0
	d_y [mm]	0	1	0	0
	d_z [mm]	0	0	-	0.1
test 5	d_x [mm]	0	-	0.5	0
	d_y [mm]	0	0	0.5	0
	d_z [mm]	0	0	0	-

The reasons why some errors should be assumed and considered are the same as those explained in the cubic UMAT intense testing. The comparison of the results in the $10^{-4}-10^{-1}$ [Hz] frequency range yielded the error results shown in table 5.7.

Table 5.7: Orthotropic UMAT intense testing average and maximum resulting errors in a displaced node main reaction force, RF, and its loss angle, δ calculations.

		average error	maximum error
test 1	RF_1	0.2909%	0.8126%
	δ_1	1.0574%	4.7510%
test 2	RF_3	0.4128%	1.8708%
	δ_3	1.1018%	5.2516%
test 3	RF_3	0.3551%	1.5925%
	δ_3	1.3915%	6.3329%
test 4	RF_3	0.0705%	0.1176%
	δ_3	0.8354%	3.7352%
test 5	RF_2	0.6578%	2.6943%
	δ_2	1.0945%	4.5193%

The results of this simulations yield a quite low average error, with a higher maximum error, specially in the loss angle calculations. The error takes this higher values when the calculations are performed over 10^{-2} [Hz], in calculations at frequencies below such frequency the error remains generally lower than 1%, which can be considered negligible. This increased error values are mainly due to the input data inaccuracies in the (13) term described in the previous section. Despite this increased error, the UMAT behaviour is good as a maximum error of 6% is typically affordable and minor errors can be considered below $f = 10^{-2}$ [Hz].

5.3 Plane stress UMAT: DMA test

In the present section the motivation and data extraction for a plane stress UMAT is included. Furthermore, it will be applied for the simulation of a Dynamic Mechanical Analysis (DMA) on a layered composite with different configurations.

5.3.1 Motivation for the plane stress UMAT

As presented in section 4.1.1, in some cases the reduction of the dimensions of the problem is possible via plane stress theory. This reduces the computation costs as the rank of the elasticity matrix and the number of degrees of freedom are reduced.

If the orthotropic UMAT implements the procedure in section 4.1.1, seems such theory is only applicable for elastic materials, because when complex computations are carried out to compute the plane stress elasticity matrix out of the 3D one, only the complex moduli of the components gets proper results. The phase angle calculation yields in general high errors that cannot be assumed.

In order to avoid this inconvenience and to have the possibility to accurately perform plane stress calculations, a new UMAT, based on the previous orthotropic UMAT, has been developed. This UMAT has as input directly the values of the plane stress elasticity tensor, this way complex matrix transformations are avoided, as the terms for the elasticity tensor can be directly extracted from Abaqus if proper boundary conditions are chosen.

5.3.2 Material input data extraction

The material input data for the plane stress UMAT is obtained from the transversally isotropic unit cell 5.8, considering plane stress assumptions in the x-z plane. The 1 and 2 directions coincide in this case with the z and x directions respectively.

In this case, the chosen matrix material is once again the polymer used in the cubic unit cell. On the other hand, for the fiber material, boron-containing E-glass fiber with no viscoelastic properties has been considered. Its elastic properties are $E = 77{,}000$ MPa and $\nu = 0.22$. [9]

Table 5.8: Homogenized plane stress transversal isotropic material data by unit cell simulations.

f [Hz]	**11** [MPa]	δ_{11}[°]	**12** [MPa]	δ_{12}[°]	**22** [MPa]	δ_{22}[°]	**33** [MPa]	δ_{33}[°]
10^{-5}	46292.707	0.000053	155.947	0.0210	763.762	0.0129	169.018	0.0407
$5.0\cdot10^{-5}$	46292.708	0.000294	155.949	0.1156	763.764	0.0710	169.020	0.2237
10^{-4}	46292.709	0.000534	155.951	0.2103	763.768	0.1291	169.025	0.4067
$2.5\cdot10^{-4}$	46292.717	0.001335	155.971	0.5255	763.799	0.3227	169.059	1.0165
$5.0\cdot10^{-4}$	46292.747	0.002669	156.042	1.0501	763.912	0.6453	169.182	2.0317
$7.5\cdot10^{-4}$	46292.796	0.004001	156.160	1.5729	764.100	0.9675	169.387	3.0442
10^{-3}	46292.865	0.005332	156.324	2.0928	764.362	1.2892	169.673	4.0530
$1.25\cdot10^{-3}$	46292.954	0.006658	156.535	2.6091	764.698	1.6102	170.040	5.0566
$2.5\cdot10^{-3}$	46293.684	0.013216	158.253	5.1065	767.482	3.1993	173.061	9.9566
$3.75\cdot10^{-3}$	46294.869	0.019583	160.979	7.3988	772.037	4.7478	177.961	14.5657
$5.0\cdot10^{-3}$	46296.463	0.025680	164.532	9.4236	778.249	6.2389	184.557	18.7865
$6.25\cdot10^{-3}$	46298.413	0.031452	168.711	11.1516	785.974	7.6594	192.633	22.5632
$7.5\cdot10^{-3}$	46300.660	0.036858	173.317	12.5817	795.055	8.9997	201.962	25.8773
$8.75\cdot10^{-3}$	46303.148	0.041880	178.174	13.7330	805.328	10.2537	212.322	28.7383
10^{-2}	46305.822	0.046510	183.136	14.6356	816.634	11.4184	223.508	31.1742
$2.0\cdot10^{-2}$	46329.526	0.071158	218.349	16.5662	928.848	17.7002	325.364	39.9843

Continued on next page

Table 5.8 – *Continued from previous page*

f [Hz]	**11** [MPa]	δ_{11}[º]	**12** [MPa]	δ_{12}[º]	**22** [MPa]	δ_{22}[º]	**33** [MPa]	δ_{33}[º]
$3.0 \cdot 10^{-2}$	46351.237	0.080848	241.422	15.2403	1049.325	19.9633	422.336	39.7695
$4.0 \cdot 10^{-2}$	46368.804	0.082859	256.079	13.5531	1156.042	20.0639	501.575	36.9802
$5.0 \cdot 10^{-2}$	46382.548	0.081027	265.775	12.0280	1242.800	19.1848	562.805	33.6665
$6.0 \cdot 10^{-2}$	46393.179	0.077378	272.455	10.7326	1310.684	17.9451	609.175	30.4942
$7.0 \cdot 10^{-2}$	46401.391	0.073004	277.214	9.6458	1363.097	16.6367	644.199	27.6587
$8.0 \cdot 10^{-2}$	46407.761	0.068487	280.699	8.7326	1403.554	15.3858	670.817	25.1875
$9.0 \cdot 10^{-2}$	46412.744	0.064118	283.310	7.9608	1434.982	14.2394	691.256	23.0514
10^{-1}	46416.679	0.060030	285.308	7.3035	1459.627	13.2087	707.135	21.2057
$1.25 \cdot 10^{-1}$	46423.439	0.051255	288.612	6.0307	1501.455	11.0972	733.754	17.5816
$2.5 \cdot 10^{-1}$	46434.018	0.028269	293.366	3.1699	1562.893	5.9703	770.762	9.3064
$3.75 \cdot 10^{-1}$	46435.898	0.019267	293.906	2.1467	1568.052	4.0575	770.779	6.3362
$5.0 \cdot 10^{-1}$	46436.156	0.014606	293.591	1.6303	1560.827	3.0819	761.723	4.8451
$6.25 \cdot 10^{-1}$	46435.807	0.011782	292.876	1.3221	1547.445	2.4963	747.506	3.9641
$7.5 \cdot 10^{-1}$	46435.105	0.009898	291.871	1.1194	1529.492	2.1092	729.114	3.3937
$8.75 \cdot 10^{-1}$	46434.131	0.008560	290.608	0.9776	1507.513	1.8367	706.879	3.0045
1.0	46432.911	0.007565	289.090	0.8744	1481.727	1.6366	680.928	2.7318

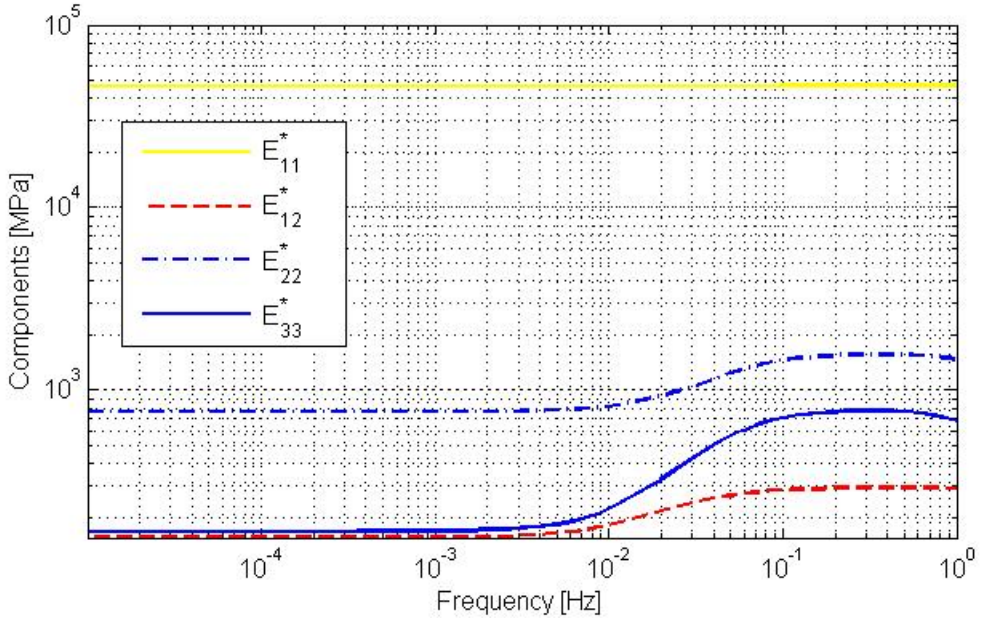

Figure 5.11: Plane stress transversally isotropic elasticity matrix components input data in graphical form.

Two z-direction tensile tests with restrained x-displacement and one x-direction tensile test with reastrained z-displacement were carried out to get terms (11), (12) and (22) respectively. Furthermore an in-plane shear test is applied to get the remaining (33) term. All of them are performed at different frequencies as in the previous cases. The computation strategy and UMAT structure is the same applied in the orthotropic case.

The resulting transversally isotropic, plane stress input data are presented in table 5.8 and graphically represented in figures 5.11 and 5.12.

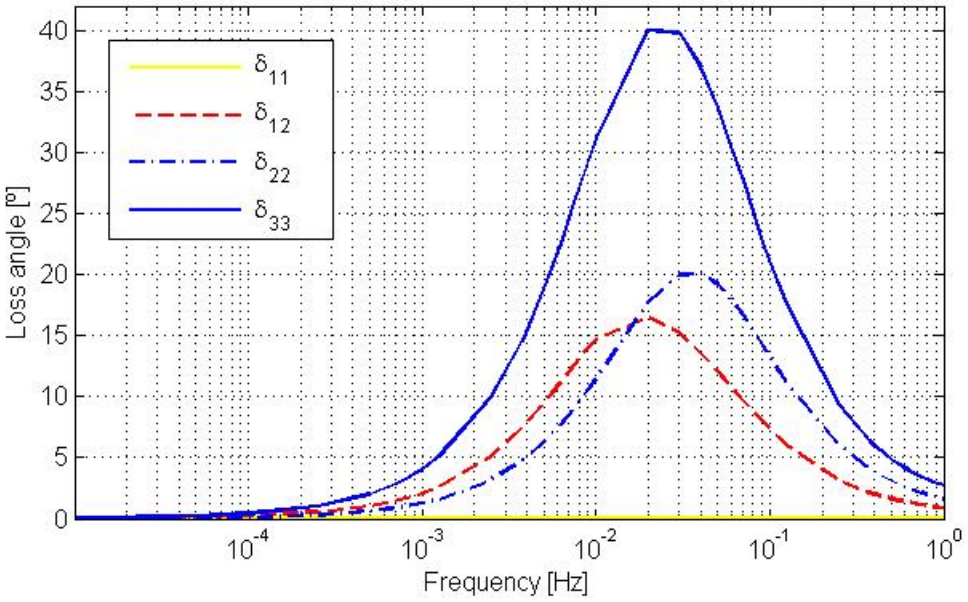

Figure 5.12: Plane stress transversally isotropic loss angle input data in graphical form.

5.3.3 DMA application

In the present section the plane stress UMAT with the transversally isotropic material input data of the previous section will be applied to a model for Dynamic Mechanical Analysis, also developed in the context of the present thesis.

DMA description and applications

Dynamic Mechanical Analysis, otherwise known as DMA, is a technique where a small deformation is applied to a sample in a cyclic manner. This allows the materials response to stress, temperature, frequency and other values to be studied. The term DMA is also used to refer to the machine that performs the test.

DMA works by applying a sinusoidal deformation to a sample of known geometry. The sample can be subjected by a controlled stress or a controlled strain. For a known stress, the sample will then deform a certain amount. How much it deforms is related to its stiffness. A force motor is used to generate the sinusoidal wave and this is transmitted to the sample via a drive shaft. An example of a DMA machine is represented in figure 5.13.

DMA measures stiffness and damping, these are reported as modulus and $\tan\delta$, which as

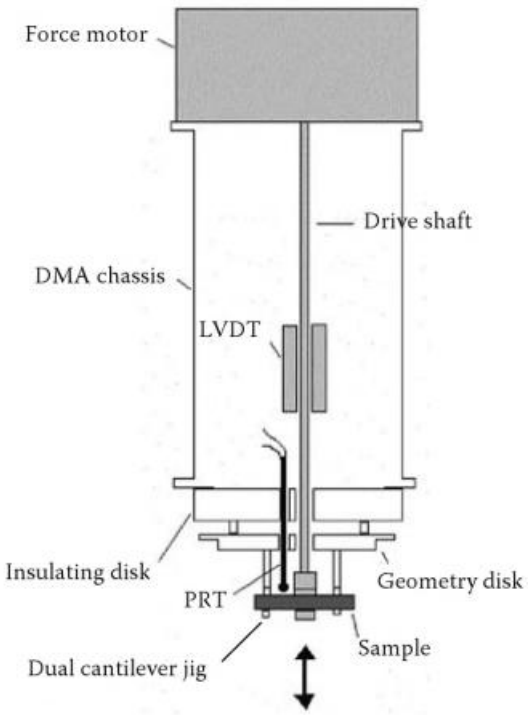

Figure 5.13: Schematic of the PerkinElmer DMA 8000. [19]

described in section 2.2.2, is a measure of damping or energy dissipation of the material. So it is most useful for studying the viscoelastic behavior of materials.

The temperature of the sample or the *frequency* of the stress are often varied, leading to variations in the complex modulus; this approach can be used to describe viscoelastic properties, to locate the glass transition temperature of the material or to identify transitions corresponding to other molecular motions.

Model description and application

A sample of 10 mm width, 50 mm support distance and 1 mm thickness has been chosen for the DMA model. The model includes a four layered section definition, so each layer consists in a 0.25 mm thickness ply with the possibility to set up different material orientations to each layer. The model is represented in figure 5.14.

Such Abaqus model consists in a three point load case with a periodic central displacement of 40 μm. The selected element type has been the thin shell element S4R5, which is applicable as the ratio thickness to support distance is very low. The reason for this selection is that the trans-

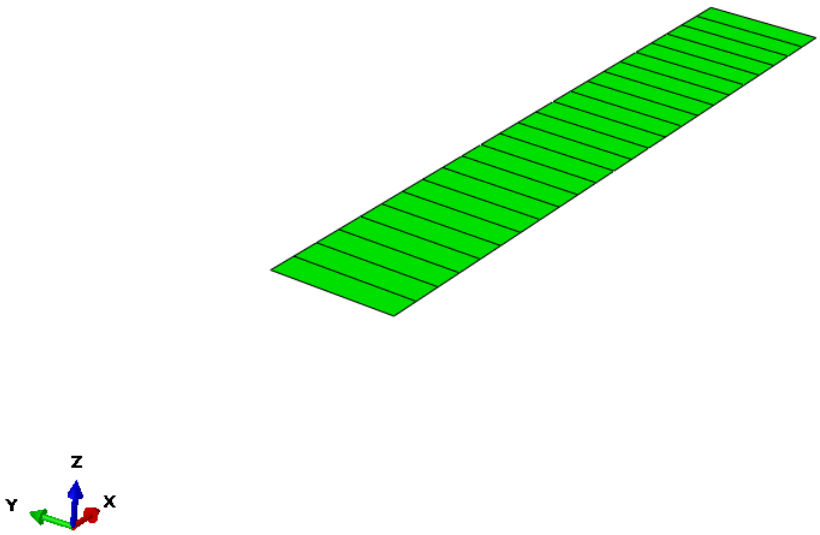

Figure 5.14: DMA Abaqus model.

verse shear stiffness, required by Abaqus for performing its computations with shell elements, has no influence in the simulation results. The proper calculation of such material parameter is quite complex as the material is non-homogeneous, with the S4R5 such complications are avoided.

Different simulations have been performed in order to compare the behaviour of different configurations of the four layered composite. Such simulations consist in steady state dynamic analysis at different frequencies in the $10^{-5} - 10^{-2}$ [Hz] frequency range. The studied layer configurations are $[0]_4$, $[90]_4$, $[\pm 45]_2$, $[90/0]_s$ and $[0/90]_s$. An example of how the deformed shape looks like is included in figures 5.15 and 5.16.

Simulation results

For each configuration and at different frequencies, the reaction force in the 3rd direction and its loss angle at the loading point has been predicted. The results are presented in table 5.9 and graphically represented in figures 5.17 and 5.18.

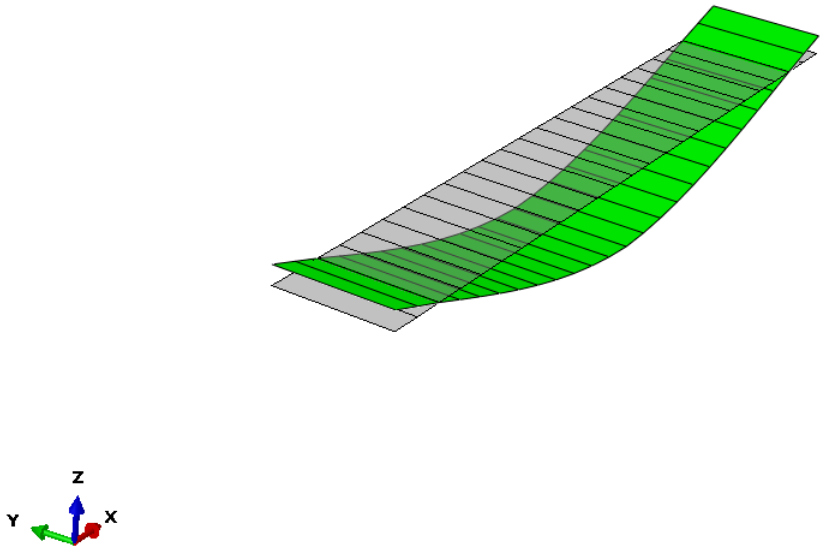

Figure 5.15: DMA deformed model. $[0]_4$ composite, $f = 10^{-5}$ [Hz], scale factor = 150.

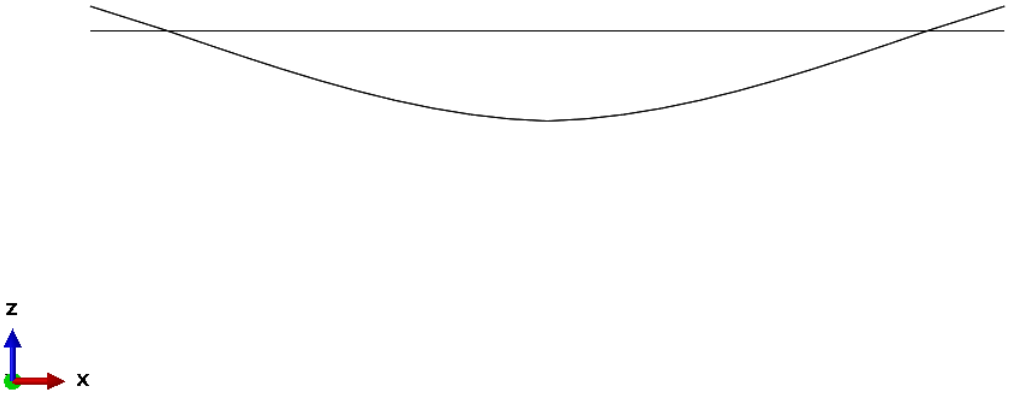

Figure 5.16: DMA deformed model. 2D view of x-z plane. $[0]_4$ composite, $f = 10^{-5}$ [Hz], scale factor = 150.

Table 5.9: RF and δ simulation results for the different layer configurations in the 3-direction at the load point in the DMA test.

	$[0]_4$		$[90]_4$		$[\pm 45]_2$		$[90/0]_s$		$[0/90]_s$	
f [Hz]	RF_3 [10^{-3} N]	δ_3[°]	RF_3 [10^{-3} N]	δ_3[°]	RF_3 [10^{-3} N]	δ_3[°]	RF_3 [10^{-3} N]	δ_3[°]	RF_3 [10^{-3} N]	δ_3[°]
10^{-5}	527.932	0.00003	9.7739	0.01286	8.5126	0.03991	81.4086	0.00136	469.667	0.00007
$2.5\cdot10^{-5}$	527.932	0.00008	9.7740	0.03457	8.5127	0.10727	81.4087	0.00365	469.667	0.00019
$5.0\cdot10^{-5}$	527.932	0.00016	9.7743	0.07075	8.5131	0.21952	81.4090	0.00746	469.668	0.00040
$7.5\cdot10^{-5}$	527.933	0.00023	9.7748	0.09968	8.5137	0.30930	81.4095	0.01052	469.668	0.00056
10^{-4}	527.933	0.00030	9.7755	0.12861	8.5145	0.39905	81.4102	0.01357	469.669	0.00072
$2.0\cdot10^{-4}$	527.939	0.00059	9.7805	0.25708	8.5204	0.79755	81.4152	0.02714	469.674	0.00144
$3.0\cdot10^{-4}$	527.947	0.00089	9.7888	0.38527	8.5300	1.19492	81.4234	0.04070	469.683	0.00216
$4.0\cdot10^{-4}$	527.959	0.00119	9.8004	0.51306	8.5435	1.59074	81.4350	0.05426	469.695	0.00288
$5.0\cdot10^{-4}$	527.975	0.00148	9.8152	0.64036	8.5602	1.98480	81.4497	0.06781	469.710	0.00360
$6.0\cdot10^{-4}$	527.994	0.00178	9.8336	0.76690	8.5817	2.37567	81.4679	0.08134	469.729	0.00432
$7.0\cdot10^{-4}$	528.016	0.00208	9.8551	0.89272	8.6063	2.76394	81.4893	0.09487	469.751	0.00504
$8.0\cdot10^{-4}$	528.042	0.00237	9.8799	1.01757	8.6348	3.14845	81.5140	0.10838	469.777	0.00575
$9.0\cdot10^{-4}$	528.071	0.00267	9.9082	1.14137	8.6674	3.52881	81.5421	0.12186	469.807	0.00647
10^{-3}	528.104	0.00296	9.9396	1.26408	8.7031	3.90539	81.5733	0.13534	469.839	0.00719
$2.0\cdot10^{-3}$	528.622	0.00591	10.4430	2.39778	9.2854	7.30589	82.0703	0.26814	470.356	0.01429
$3.0\cdot10^{-3}$	529.485	0.00880	11.2886	3.30946	10.2352	9.91734	82.8962	0.39676	471.218	0.02125
$4.0\cdot10^{-3}$	530.694	0.01163	12.4968	3.94635	11.5645	11.61918	84.0550	0.51939	472.424	0.02804

Continued on next page

Table 5.9 – *Continued from previous page*

	$[0]_4$		$[90]_4$		$[\pm 45]_2$		$[90/0]_s$		$[0/90]_s$	
f [Hz]	RF_3 [10^{-3} N]	δ_3[º]	RF_3 [10^{-3} N]	δ_3[º]	RF_3 [10^{-3} N]	δ_3[º]	RF_3 [10^{-3} N]	δ_3[º]	RF_3 [10^{-3} N]	δ_3[º]
$5.0 \cdot 10^{-3}$	532.250	0.01438	14.0946	4.29530	13.2829	12.44565	85.5504	0.63445	473.976	0.03460
$6.0 \cdot 10^{-3}$	534.155	0.01705	16.1229	4.35910	15.4200	12.46272	87.3904	0.73923	475.878	0.04080
$7.0 \cdot 10^{-3}$	536.411	0.01962	18.6265	4.16996	17.9787	11.86885	89.5771	0.83381	478.128	0.04669
$8.0 \cdot 10^{-3}$	539.020	0.02208	21.6686	3.74961	20.9820	10.79240	92.1176	0.91754	480.729	0.05225
$9.0 \cdot 10^{-3}$	541.983	0.02445	25.3289	3.11190	24.4546	9.33803	95.0203	0.98999	483.684	0.05747
10^{-2}	545.304	0.02672	29.7080	2.26028	28.4219	7.58756	98.2950	1.05093	486.996	0.06233

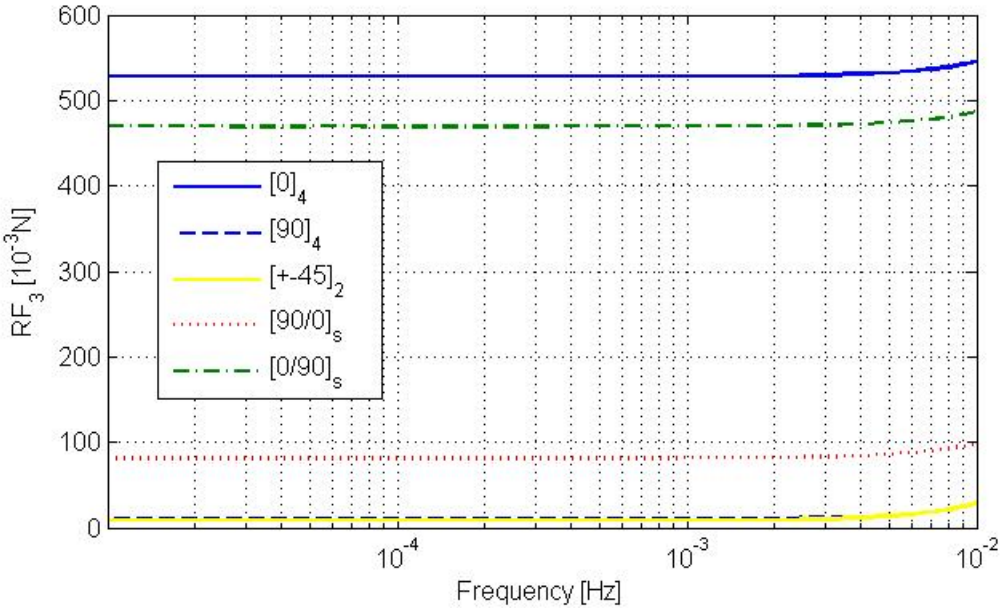

Figure 5.17: DMA RF_3 results in graphical form.

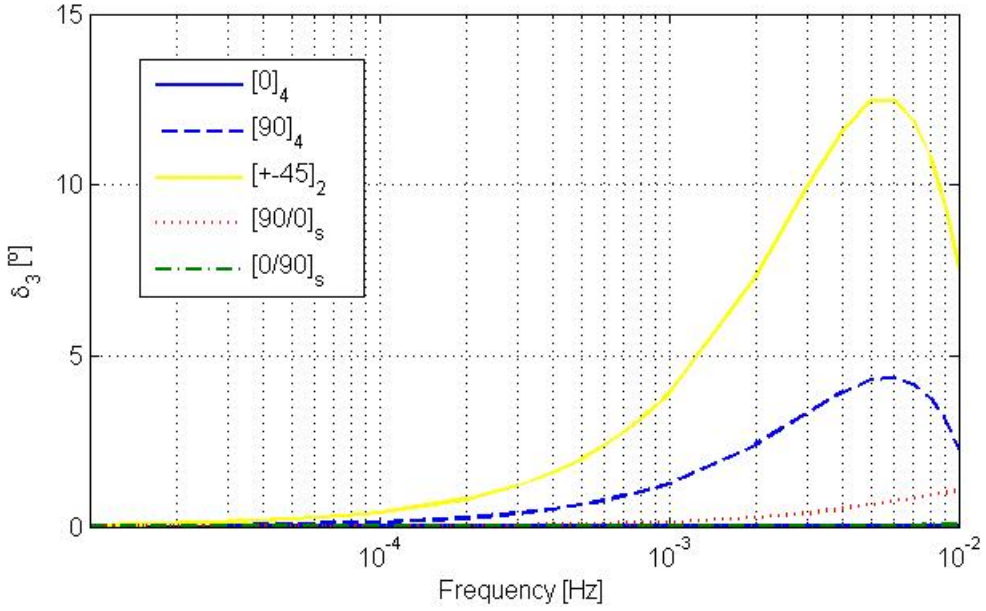

Figure 5.18: DMA δ_3 results in graphical form.

Looking at the reaction force in the third direction at the loading point, RF_3, graphically represented in figure 5.17, the results from the DMA simulations yielded, as expected, that the stiffest layer configuration is the $[0]_4$, followed by the $[0/90]_s$ one. In contrast, the $[90]_4$ and the

$[\pm 45]_2$ configurations are reflected as the most flexible ones.

On the other hand, on the shift angle representation in figure 5.18, we can appreciate that those configurations with higher stiffness present practically no damping, as the loss angle remains much closer to zero than in the softer cases. This is consequence of the fiber properties. The behaviour of the stiffer configurations is mainly influenced by the fiber material, which has no viscoelastic properties. Also the percentage increase in the reaction force in the high loss angle frequency range, which is quite accused in the case of the the $[90]_4$ and the $[\pm 45]_2$ configurations, is almost negligible in the $[0]_4$ and the $[0/90]_s$ cases.

Chapter 6

Summary

Three different Abaqus UMATs have been successfully developed in the present thesis, one for cubic anisotropy, another one to orthotropy and one last one to deal with plane stress cases. Such UMATs yielded good results in those cases where the input data was correctly selected. In consequence, the simulation of orthotropic, and less complex types of material symmetries, linear viscoelastic materials in the frequency domain is possible in Abaqus through the application of the developed UMATs.

Furthermore, the increase in computational efficiency in those cases where homogenization was applied has been proved, with a computation time reduction up to 95

Last but not least, the development of the DMA model allows the simulation of a Dynamic Mechanical Analysis, which is usually applied in material characterization, without having the physic machine and the finite sample to experimentally perform it.

Further investigation

There are two main further investigation directions. On one hand, one path could be the study of the complex matrix conversion from the 3D to the plane stress case. On the other hand is the experimental DMA application to a finite sample and its comparison to the Abaqus DMA model results, in order to prove its accuracy and its strong and weak points.

Appendix A

UMAT interface

The present appendix is an extract of the DS Simulia ABAQUS 6.14 User's Guide [1]. It includes the UMAT interface structure and a further explanation of the most important terms or variables that take part in the frequency domain linear viscoelastic UMAT programming.

A.1 UMAT interface structure

```
      SUBROUTINE UMAT(STRESS,STATEV,DDSDDE,SSE,SPD,SCD,
     1 RPL,DDSDDT,DRPLDE,DRPLDT,
     2 STRAN,DSTRAN,TIME,DTIME,TEMP,DTEMP,PREDEF,DPRED,CMNAME,
     3 NDI,NSHR,NTENS,NSTATV,PROPS,NPROPS,COORDS,DROT,PNEWDT,
     4 CELENT,DFGRD0,DFGRD1,NOEL,NPT,LAYER,KSPT,JSTEP,KINC)
C
      INCLUDE 'ABA_PARAM.INC'
C
      CHARACTER*80 CMNAME
      DIMENSION STRESS(NTENS),STATEV(NSTATV),
     1 DDSDDE(NTENS,NTENS),DDSDDT(NTENS),DRPLDE(NTENS),
     2 STRAN(NTENS),DSTRAN(NTENS),TIME(2),PREDEF(1),DPRED(1),
     3 PROPS(NPROPS),COORDS(3),DROT(3,3),DFGRD0(3,3),DFGRD1(3,3),
     4 JSTEP(4)
```

```
    user coding to define DDSDDE, STRESS, STATEV, SSE, SPD, SCD
    and, if necessary, RPL, DDSDDT, DRPLDE, DRPLDT, PNEWDT
    RETURN
    END
```

A.2 Variable list

`DDSDDE(NTENS,NTENS)`

For viscoelastic behavior in the frequency domain, the Jacobian matrix must be dimensioned as `DDSDDE(NTENS,NTENS,2)`. The stiffness contribution (storage modulus, $E_{(ij),s}$) must be provided in `DDSDDE(NTENS,NTENS,1)`, while the damping contribution (loss modulus, $E_{(ij),l}$) must be provided in `DDSDDE(NTENS,NTENS,2)`.

`TIME(1)`

Value of step time at the beginning of the current increment or frequency.

`NDI`

Number of direct stress components at this point.

`NSHR`

Number of engineering shear stress components at this point.

`NTENS`

Size of the stress or strain component array (`NDI` + `NSHR`).

`PROPS(NPROPS)`

User-specified array of material constants associated with this user material.

`NPROPS`

User-defined number of material constants associated with this user material.

Appendix B

Material data input

If a UMAT subroutine is used, the material parameters should be passed in to Abaqus as input data in the user material definition. In this appendix the formatting of the data that should be provided will be dealt for the cubic, the orthotropic and the plane stress UMATs.

B.1 Cubic UMAT data input

In cubic symmetry three complex moduli are needed. Therefore, six values should be passed in as input at each frequency. The selected material input data is explained in section 5.1.1.

The order of the input data should be, frequency of the following six material data input, complex bulk modulus K^*, its loss angle, δ_K, the complex shear modulus G^*, its loss angle, δ_G, the complex shear modulus M^* and its loss angle, δ_M. Every loss angle must be specified in degrees. Finally, as Abaqus reads eight values per input data line, a zero value should be input as the eighth input at each frequency. Afterwards, in case it exists, the next frequency with its correspondent material data should be typed.

In conclusion, the number of material input data should be $8n_f$, with n_f the number of frequencies the user has material data input available.

User defined cubic material input example

Here is an example of cubic material input data where material properties are specified at three different frequencies.

```
*MATERIAL, NAME=VISCO
*USER MATERIAL, CONSTANTS=24
1.0E-3, 1.943, 3.655, 2.332, 3.831, 0.139, 3.646, 0.
5.0E-5, 2.235, 18.23, 2.541, 20.98, 0.154, 16.25, 0.
1.0E-2, 2.527, 27.26, 3.046, 29.03, 0.174, 27.35, 0.
```

B.2 Orthotropic UMAT data input

In orthotropic symmetry nine complex moduli are needed. Therefore, 18 values should be passed in as input at each frequency. The selected material input data are explained in section 5.2.1.

In this case again the first input data should be the frequency of the following 18 material data input. The order of the matrix terms input data at that frequency is as follows, term (11), (12), (13), (22), (23), (33), (44), (55), (66). For each term of the elasticity matrix its complex module and its respective loss angle in degrees should be given in this order. Once again, as Abaqus reads eight values per input data line, five zero values should be input in order to complete the line at each frequency. Afterwards, in case it exists, the next frequency with its correspondent material data should be typed.

In conclusion, the number of material input data should be $19n_f$, with n_f the number of frequencies the user has material data input available.

User defined orthotropic material input example

Here is an example with transversally isotropic material input data where material properties are specified at two different frequencies.

```
*MATERIAL, NAME=VISCO
*USER MATERIAL, CONSTANTS=48
3.00E-002, 53.988, 26.549, 28.012, 22.551, 27.336, 1.671, 53.988
26.549, 27.336, 1.671, 122.191, 27.283, 13.057, 30.838, 26.307
40.250, 26.307, 40.250, 0., 0., 0., 0., 0.
```

```
4.00E-002, 60.063, 24.028, 30.566, 20.137, 27.356, 5.086, 60.063
24.028, 27.356, 5.086, 136.525, 24.904, 14.818, 28.043, 31.307
37.525, 31.307, 37.525, 0., 0., 0., 0., 0.
```

B.3 Plane stress UMAT data input

In plane stress linear viscoelasticity, a orthotropic material needs 4 complex moduli to be defined. Therefore, 8 values should be passed in as input at each frequency. In this case the selected material input data are explained in section 5.3.2.

As in the other UMATs, the first input data should be the frequency of the following 8 material data input. The order of the matrix terms input data at that frequency is as follows, term (11), (12), (22), and (33). As in the orthotropic UMAT, for each term of the elasticity matrix its complex module and its respective loss angle in degrees should be given in this order. As before, because Abaqus reads eight values per input data line, seven zero values should be input in order to complete the line at each frequency. Afterwards, in case it exists, the next frequency with its correspondent material data should be typed.

In conclusion, the number of material input data should be $9n_f$, with n_f the number of frequencies the user has material data input available.

User defined plane stress input example

Here is an example with plane stress, transversally isotropic material input data where material properties are specified at two different frequencies.

```
*MATERIAL, NAME=VISCO
*USER MATERIAL, CONSTANTS=32
4.00E-002, 46368.804, 0.0828, 256.079, 13.553, 1156.042, 20.063, 501.575
36.980, 0., 0., 0., 0., 0., 0., 0.
5.00E-002, 46382.548, 0.0810, 265.775, 12.027, 1242.800, 19.184, 562.805
33.666, 0., 0., 0., 0., 0., 0., 0.
```

Bibliography

[1] Dassault Systèmes *ABAQUS DS Simulia 6.14 Online Documentation.* (2014)

[2] Accorsi, M.L. *A method for modeling microstructural material discontinuities in a finite element analysis.* Int. J. Num. Meth. Engng., 26. 2187–2197. (1988)

[3] Banhart, J., Ashby, M.F. and Fleck, N.A. *Metal Foams and Porous Metal Structures. (1999).*

[4] Bathe, K.J. *Finite Element Procedures.* Prentice-Hall, Inc. (1996).

[5] Bauccio, M. *ASM Engineering Materials Reference Book, 2nd ed.* ASM International (Materials Park, OH). (1994).

[6] Böhm, H.J. *A short introduction to basic aspects of continuum micromechanics.* ILSB Report 206, Institute of Lightweight Design and Structural Biomechanics, TU Vienna. 69-84. (2014)

[7] Böhm, H.J. and Han, W. *Comparisons between three-dimensional and twodimensional multi-particle unit cell models for particle reinforced metal matrix composites.* Modelling Simul. Mater. Sci. Eng. 47-65. (2001)

[8] Bower, A.F. *Applied Mechanics of Solids.* CRC Press. Taylor & Francis Group. 81-87. (2009)

[9] Donaldson, S. L. and Miracle, D. B. *ASM Handbook Composites Volume 21.* ASM International. (2001)

[10] Gassner, C. and Pettermann, H. *Dämpfungsverhalten viskoelastischer, zellulärer Strukturen.* Institut für Leichtbau und Struktur-Biomechanik (ILSB), Technische Universität Wien (2011).

[11] Gibson, L. and Ashby, M.F. *Cellular Solids: Structure and Properties.* Pergamon Press. (1988).

[12] Ghosh, S., Lee, K.H., and Moorthy, S. *Two scale analysis of heterogeneous elastic-plastic materials with asymptotic homogenization and Voronoi cell finite element model.* Comput. Meth. Appl. Mech. Engng., 132. 63–116. (1996).

[13] Gross, D., Hauger, W. and Wriggers, P. *Technische Mechanik: Band 4. (2004).*

[14] Gusev, A.A. *Representative volume element size for elastic composites: a numerical study.* J. Mech. Phys. Solids 45. 1449-1459. (1997).

[15] *http://medicalpicturesinfo.com/cancellous-bone/* on 09/03/2015.

[16] *http://www.virginia.edu/ms/research/wadley/celluar-materials.html* on 02/05/2015.

[17] Irwin, J. D. *Basic Engineering Circuit Analysis.* New York: Macmillan. (1989).

[18] Lakes, R. *Viscoelastic Materials.* Cambridge University Press. 1-111. (2009).

[19] Menard, K. P. *Dynamic Mechanical Analysis: A Practical Introduction.* CRC Press. 1-12. (2008).

[20] Meyers, M.A. and Chawla, K.K. *Mechanical Behavior of Materials.* Cambridge University Press. 98-103. (1999).

[21] Michel, J.C., Moulinec, H. and Suquet, P. *Composites à microstructure périodique.* In Bornert, M., Bretheau, T. and Gilormini, P. editors, Homogénéisation en mécanique des matériaux 1. Matériaux aléatoires élastiques et milieux périodiques. 57–94. (2001).

[22] Moës, N., Cloirec, M., Cartraud, P. and Remacle, J.F. *A computational approach to handle complex microstructure geometries.* Comput. Meth. Appl. Mech. Engng. 192. 3163–3177. (2003).

[23] Nye, J.F. *Physical Properties of Crystals. Their Representation by Tensors and Matrices* Clarendon Press, Oxford. 131-149. (1985).

[24] Pahr, D.H. and Böhm, H.J. *Assessment of mixed uniform boundary conditions for predicting the mechanical behavior of elastic and inelastic discontinuously reinforced composites.* Comput.Model.Engng.Sci., 34. 117–136, 2008.

[25] Pettermann, H.E. *A comprehensive unit cell model: a study of coupled effects in piezoelectric 1–3 composites* Department of Materials Science and Engineering, Massachusetts Institute of Technology, Cambridge, MA 02139, USA. (2000).

[26] Pettermann, H.E. *Viscoelastic Mechanical Properties of Cellular Materials and Structures — the Development of an ABAQUS UMAT* Institute of Lightweight Design and Structural Biomechanics. Vienna University of Technology. (2010).

[27] Pettermann, H.E. and Hüsing, J. *Modeling and simulation of relaxation in viscoelastic open cell materials and structures* Institute of Lightweight Design and Structural Biomechanics. Vienna University of Technology. (2012).

[28] Quilici, S. and Cailletaud, G. *FE simulation of macro-, meso- and microscales in polycrystalline plasticity.* Comput. Mater. Sci., 16. 383–390. (1999).

[29] Stampfl, J., Seyr, M.M., Luxner, M.H., Pettermann, H.E., Woesz, A. and Fratzl, P. *Regular, Low Density Cellular Structures Rapid Prototyping, Numerical Simulation, Mechanical Testing.* In: Landis, W.J., Orme, C., Wang, R. (Eds.), Mater. Res. Soc. Symp. Proc, San Francisco, USA. (2004).

[30] Terada, K., Miura, T. and Kikuchi, N. *Digital image-based modeling applied to the homogenization analysis of composite materials.* Comput. Mech., 20. (1997).

[31] Zeman, J. and Sejnoha, M. *Numerical evaluation of effective elastic properties of graphite fiber tow impregnated by polymer matrix.* J. Mech. Phys. Sol., 49. 69-90. (2001).

[32] Zienkiewicz, O.C. and Taylor, R.L. *The Finite Element Method. Volume 1: Solid Mechanics.* Butterworth-Heinemann. 1-16. (2000).

[33] Zienkiewicz, O.C. and Taylor, R.L. *The Finite Element Method. Volume 2: Solid Mechanics.* Butterworth-Heinemann. 39-48. (2000).